2012

The Radiation Quality Factor Of Vertically Polarized Spherical Antennas Above A Conducting Ground Plane

Hsieh-chi Chang
University of Massachusetts Amherst

THE RADIATION QUALITY FACTOR OF VERTICALLY POLARIZED SPHERICAL ANTENNAS ABOVE A CONDUCTING GROUND PLANE

A Thesis Presented

by

HSIEH-CHI CHANG

Submitted to the Graduate School of the University of Massachusetts Amherst in partial fulfillment of the requirements for master of

MASTER OF SCIENCE IN ELECTRICAL AND COMPUTER ENGINEERING

September 2012

Electrical and Computer Engineering

THE RADIATION QUALITY FACTOR OF VERTICALLY POLARIZED SPHERICAL ANTENNAS ABOVE A CONDUCTING GROUND PLANE

A Thesis Presented

by

HSIEH-CHI CHANG

Approved as to style and content by

Do-Hoon Kwon, Chair

Ramakrishna Janaswamy, Member

David M. Pozar, Member

Christopher V. Hollot, Department Head
Electrical and Computer Engineering

ACKNOWLEDGMENTS

I'd like to express my gratitude to Prof. Yong Heui Cho of Mokwon University, Korea for his guidance in the initial stage of this research. I also want to thank my advisor Prof. Do-Hoon Kwon. I would not have been able to finish the thesis work without his guidance. He always points me in the right direction. I also want to thank Mary McKay for her encouragement to finish the thesis. I am grateful to Prof. Pozar and Prof. Janaswamy, my thesis committee members. Their constructive comments improved the quality of the thesis. Finally, I appreciate the support from my family and friends.

This thesis work was supported in part by The SI Organization, Inc.

ABSTRACT

THE RADIATION QUALITY FACTOR OF VERTICALLY POLARIZED SPHERICAL ANTENNAS ABOVE A CONDUCTING GROUND PLANE

SEPTEMBER 2012

HSIEH-CHI CHANG

B.Sc., NATIONAL CHIAYI UNIVERISTY
M.S.E.C.E. UNIVERSITY OF MASSACHUSETTS AMHERST

Directed by: Professor Do-Hoon Kwon

The radiation quality factor of small vertically polarized antennas above a ground plane is investigated. Although the quality factor of small antennas in free space has been investigated extensively in the past, the exact effect of a conducting ground plane on the antenna bandwidth is not clearly understood. In this thesis, quality factors of vertically polarized antennas above a ground plane are computed and compared with their free-space counterparts. The theoretical results on quality factors are validated with simulations of electrically small spherical helix antennas.

TABLE OF CONTENTS

Page

LIST OF TABLES

Table **Page**

LIST OF FIGURES

Figure **Page**

CHAPTER 1

INTRODUCTION

Electrically small antennas have been an important research topic for many years. The interest in this field is increasing with the development of broadband antennas in small sizes. The radiation quality factor Q is an important measure and research topic in electrically small antenna field. For electrically small antennas, only the fundamental mode of current can be assumed to flow over a spherical circumscribing surface. It is also known when the quality factor is much larger than unity, the impedance bandwidth is approximately equal to the reciprocal of the quality factor. Wheeler [1] is the first author who established the link between antenna, bandwidth, and efficiency. He used the term "radiation power factor" in studying the limitation of small antennas. The work of Chu [2] in deriving the fundamental limitation for electrically small omni-directional antennas is widely used. He considered a hypothetical sphere enclosing an electrically small antenna, where the sphere's diameter being smaller than a wavelength. In his work, the minimum Q was obtained for each TM mode. For the lowest TM_n mode, the well-known exact result is

$$Q = \frac{1}{ka} + \frac{1}{(ka)^3}, \tag{1}$$

where $k=2\pi/\lambda$ is the free-space wavenumber and a is the radius of the sphere.

Kim [3], [4] used the current on the antenna surface to model small antennas with quality factors that approach the Chu's limit. However, it was realized that the energy inside sphere was not easy to cancel. This energy should be included when the quality factor is computed in order to model practical antennas. In addition, the minimum Q should be higher than the Chu's limit, as the stored energy inside the sphere was not included by Chu. Thal [5] used a wire antenna deployed over the surface of a hypothetical sphere. He also used the Chu ladder network, and gave numerical results but no formulas. Hansen and Collin [6] included the stored energy for general TM modes and recomputed the Chu formula. Incorporating the internal stored energy, an approximate formula for the minimum Q for the lowest TM_{01} mode was also developed. It is given by [6]

$$Q_{H-C} \approx \frac{0.71327}{ka} + \frac{1.49589}{(ka)^3}. \tag{2}$$

This quality factor applies only to a spherical antenna with air core excited by an electric surface current.

Best[7], [8] used 4-arm folded spherical helix antennas to realize that the fundamental sinusoidal mode current flow on the surface. The tuned antenna's quality factor can also

be determined directly from the antenna's untuned feed point impedance [9],

$$Q(\omega_0) = \frac{\omega_0}{2R(\omega_0)} \sqrt{R'(\omega_0)^2 + \left[X'(\omega_0) + \frac{|X(\omega_0)|}{\omega_0} \right]^2}, \qquad (3)$$

where ω_0 is the tuned radian frequency, $R(\omega)$ and $X(\omega)$ are the frequency dependent feed point resistance and reactance respectively, and $R'(\omega)$ and $X'(\omega)$ are their frequency derivatives.

The vast majority of small antenna research treats antennas in free space. Chu did not consider the stored energy inside the volume and Thal added this energy into his quality factor, all limited to free-space antennas. Sten *et al*. [10] investigated the radiation Q of a combination of vertical and horizontal point diploes above a PEC ground plane. However, they considered the minimum sphere that encloses both the original antenna and the image antenna after applying the image theory. Then, Chu's approach, *i.e.* excluding the stored energy in this sphere, was used to compute the Q of the system. Hence, this approach results in very conservative Q values that cannot be closely approached in practice, thereby reducing the utility of the derived bound. This thesis will show the detail and method for quality factor of a conductor-backed small antenna in Chapter 3.

CHAPTER 2

REVIEW OF ANTENNA QUALITY FACTOR IN FREE SPACE

2.1 Spherical Wave Function

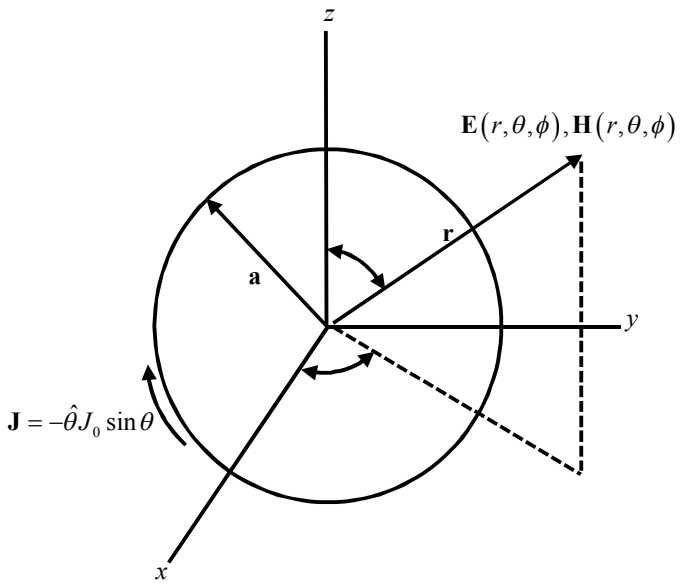

Figure 1: Coordinate system definition for an electric surface current over a sphere of radius *a* centered at *O*.

We start to solve this problem with a spherical antenna in free space, as shown in Figure 1. Using the vector spherical harmonic [11], $\mathbf{M}_{mn}^{(c)}(r,\theta,\phi)$ and $\mathbf{N}_{mn}^{(c)}(r,\theta,\phi)$, are given by

$$\mathbf{M}_{mn}^{(c)}\left(r,\theta,\phi\right)=-\hat{\theta}\,jz_n^{(c)}\left(kr\right)\frac{mP_n^m\left(\cos\theta\right)}{\sin\theta}e^{jm\phi}-\hat{\phi}z_n^{(c)}\left(kr\right)\frac{dP_n^m\left(\cos\theta\right)}{d\theta}e^{jm\phi} \qquad (4)$$

$$\begin{aligned}&\mathbf{N}_{mn}^{(c)}(r,\theta,\phi)\\&=\hat{r}\frac{n(n+1)}{kr}z_n^{(c)}(kr)P_n^m(\cos\theta)e^{jm\phi}+\hat{\theta}\frac{1}{kr}\frac{d}{d(kr)}[krz_n^{(c)}(kr)]\frac{dP_n^m(\cos\theta)}{d\theta}e^{jm\phi}\\&\quad-\hat{\phi}j\frac{1}{kr}\frac{d}{d(kr)}[krz_n^{(c)}(kr)]\frac{mP_n^m(\cos\theta)}{\sin\theta}e^{jm\phi}\end{aligned}\tag{5}$$

where $z_n^{(c)}(kr)$ is the radial function of a type specified by c. They are equal to

$$\begin{aligned}&z_n^{(1)}(kr)=j_n(kr)\\&z_n^{(2)}(kr)=y_n(kr)\\&z_n^{(3)}(kr)=h_n^{(1)}(kr)=j_n(kr)+jy_n(kr)\\&z_n^{(4)}(kr)=h_n^{(2)}(kr)=j_n(kr)-jy_n(kr)\\&m,n=0,1,2,\cdots\end{aligned}\tag{6}$$

and the field may be cast in a compact form as

$$\mathbf{E}(r,\theta,\phi)=\sum_{n=0}^{\infty}\sum_{m=-n}^{n}\left[a_{mn}\vec{M}_{mn}^{(c)}(r,\theta,\phi)+b_{mn}\vec{N}_{mn}^{(c)}(r,\theta,\phi)\right]\tag{7}$$

$$\mathbf{H}(r,\theta,\phi)=\frac{j}{\eta_0}\sum_{n=0}^{\infty}\sum_{m=-n}^{n}[a_{mn}\vec{N}_{mn}^{(c)}(r,\theta,\phi)+b_{mn}\vec{M}_{mn}^{(c)}(r,\theta,\phi)]\tag{8}$$

where η_0 is the intrinsic impedance of free space, which are valid in both near and far zones. Here, $P_n^m(cos\theta)$ denotes the associated Legendre function. Outside the sphere ($r>a$), radiation propagating wave behavior is chosen (c=4). In $\mathbf{M}_{mn}^{(4)}(r,\theta,\phi)$ and $\mathbf{N}_{mn}^{(4)}(r,\theta,\phi)$, $z_l^{(4)}(kr)=h_l^{(2)}(kr)$ is the spherical Hankel function of the second kind. Because the current which flows on the surface is the fundamental mode, it implies m=0 and n=1.

Vector spherical harmonics and the associated fields are

$$\mathbf{M}_{01}^{(4)}(r,\theta,\phi)=-\hat{\phi}h_1^{(2)}(kr)\frac{dP_1(\cos\theta)}{d\theta}=-\hat{\phi}h_1^{(2)}(kr)P_1^1(\cos\theta)\tag{9}$$

$$\begin{aligned}\mathbf{N}_{01}^{(4)}(r,\theta,\phi) &= \hat{r}\frac{2}{kr}h_1^{(2)}(kr)P_1(\cos\theta)+\hat{\theta}\frac{1}{kr}\frac{d}{d(kr)}[krh_1^{(2)}(kr)]\frac{dP_1(\cos\theta)}{d\theta} \\ &= \hat{r}\frac{2}{kr}h_1^{(2)}(kr)P_1(\cos\theta)+\hat{\theta}[h_0^{(2)}(kr)-\frac{h_1^{(2)}(kr)}{kr}]P_1^1(\cos\theta)\end{aligned} \tag{10}$$

$$\begin{aligned}&\mathbf{E}(r,\theta,\phi) \\ &= a_{01}^{r>a}\mathbf{M}_{01}^{(4)}(r,\theta,\phi)+b_{01}^{r>a}\mathbf{N}_{01}^{(4)}(r,\theta,\phi) \\ &= -a_{01}^{r>a}\hat{\phi}h_1^{(2)}(kr)P_1^1(\cos\theta) \\ &\quad + b_{01}^{r>a}\left\{\hat{r}\frac{2}{kr}h_1^{(2)}(kr)P_1(\cos\theta)+\hat{\theta}\left[h_0^{(2)}(kr)-\frac{h_1^{(2)}(kr)}{kr}\right]P_1^1(\cos\theta)\right\}\end{aligned} \tag{11}$$

$$\begin{aligned}&\mathbf{H}(r,\theta,\phi) \\ &= \frac{j}{\eta_0}\left[a_{01}^{r>a}\mathbf{N}_{01}^{(4)}(r,\theta,\phi)+b_{01}^{r>a}\mathbf{M}_{01}^{(4)}(r,\theta,\phi)\right] \\ &= \frac{j}{\eta_0}\left\{a_{01}^{r>a}\left[\hat{r}\frac{2}{kr}h_1^{(2)}(kr)P_1(\cos\theta)+\hat{\theta}\left[h_0^{(2)}(kr)-\frac{h_1^{(2)}(kr)}{kr}\right]P_1^1(\cos\theta)\right]\right. \\ &\qquad \left. - b_{01}^{r>a}\hat{\phi}h_1^{(2)}(kr)P_1^1(\cos\theta)\right\}\end{aligned} \tag{12}$$

where $a_{01}^{r>a}$ and $b_{01}^{r>a}$ are the unknown coefficients for the $r>a$ region. Inside the sphere ($r<a$), the field at the origin is finite. Therefore, c=1 is chosen. In $\mathbf{M}_{mn}^{(1)}(r,\theta,\phi)$ and $\mathbf{N}_{mn}^{(1)}(r,\theta,\phi)$, $z_l^{(1)}(kr)=j_l(kr)$ is the spherical Bessel function first kind. Vector spherical harmonics and the associated fields are

$$\mathbf{M}_{01}^{(1)}(r,\theta,\phi) = -\hat{\phi}j_1(kr)\frac{dP_1(\cos\theta)}{d\theta} = -\hat{\phi}j_1(kr)P_1^1(\cos\theta) \tag{13}$$

$$\begin{aligned}\mathbf{N}_{01}^{(1)}(r,\theta,\phi) &= \hat{r}\frac{2}{kr}j_1(kr)P_1(\cos\theta)+\hat{\theta}\frac{1}{kr}\frac{d}{d(kr)}[krj_1(kr)]\frac{dP_1(\cos\theta)}{d\theta} \\ &= \hat{r}\frac{2}{kr}j_1(kr)P_1(\cos\theta)+\hat{\theta}[j_0(kr)-\frac{j_1(kr)}{kr}]P_1^1(\cos\theta)\end{aligned} \tag{14}$$

$$
\begin{aligned}
&\mathbf{E}(r,\theta,\phi) \\
&= a_{01}^{r<a}\mathbf{M}_{01}^{(1)}(r,\theta,\phi) + b_{01}^{r<a}\mathbf{N}_{01}^{(1)}(r,\theta,\phi) \\
&= -a_{01}^{r<a}\hat{\phi}\, j_1(kr)\, P_1^1(\cos\theta) \\
&\quad + b_{01}^{r<a}\left\{\hat{r}\,\frac{2}{kr}\, j_1(kr) P_1(\cos\theta) + \hat{\theta}\left[\, j_0(kr) - \frac{j_1(kr)}{kr}\right] P_1(\cos\theta)\right\}
\end{aligned}
\tag{15}
$$

$$
\begin{aligned}
&\mathbf{H}(r,\theta,\phi) \\
&= \frac{j}{\eta_0}\left[a_{01}^{r<a}\mathbf{N}_{01}^{(1)}(r,\theta,\phi) + d_{01}\mathbf{M}_{01}^{(1)}(r,\theta,\phi)\right] \\
&= \frac{j}{\eta_0}\left\{a_{01}^{r<a}\left[\hat{r}\,\frac{2}{kr}\, j_1(kr) P_1(\cos\theta) + \hat{\theta}\left(\, j_0(kr) - \frac{j_1(kr)}{kr}\right) P_1^1(\cos\theta)\right]\right. \\
&\qquad \left. - b_{01}^{r<a}\hat{\phi}\, j_1(kr) P_1^1(\cos\theta)\right\}
\end{aligned}
\tag{16}
$$

where $a_{01}^{r<a}$ and $b_{01}^{r<a}$ are the unknown coefficients for the $r<a$ region.

Fields in the $r>a$ and $r<a$ regions should satisfy appropriate boundary conditions at $r=a$.

The tangential magnetic field is discontinuous on the boundary due to surface current distribution.

$$
\mathbf{J}_s = -\hat{\theta} J_0 \sin\theta = \hat{r} \times \mathbf{H}^t\big|_{r=a} = \hat{r} \times \left(\mathbf{H}_{r>a}^t - \mathbf{H}_{r<a}^t\right)\big|_{r=a}, \tag{17}
$$

or

$$
\begin{aligned}
&a_{01}^{r>a}\left[h_0^{(2)}(ka) - \frac{h_1^{(2)}(ka)}{ka}\right] - a_{01}^{r<a}\left[\, j_0(ka) - \frac{j_1(ka)}{ka}\right] = 0 \\
&b_{01}^{r>a} h_1^{(2)}(ka) - b_{01}^{r<a}\, j_1(ka) = -j\eta_0 J_0
\end{aligned}
\tag{18}
$$

The tangential electrical field is continuous on the boundary.

$$
\mathbf{E}_{r>a}^t\big|_{r=a} = \mathbf{E}_{r<a}^t\big|_{r=a}, \tag{19}
$$

or

$$
\begin{aligned}
&a_{01}^{r>a} h_1^{(2)}(ka) = a_{01}^{r<a} j_1(ka) \\
&b_{01}^{r>a}\left[h_0^{(2)}(ka) - \frac{h_1^{(2)}(ka)}{ka} \right] = b_{01}^{r<a}\left[j_0(ka) - \frac{j_1(ka)}{ka} \right]
\end{aligned} \tag{20}
$$

The four unknown coefficients can be found from (18) and (20) as

$$
\begin{aligned}
a_{01}^{r>a} &= a_{01}^{r<a} = 0 \\
b_{01}^{r>a} &= -j\eta_0 J_0 ka\left[kaj_1(ka) \right]' \\
b_{01}^{r<a} &= -j\eta_0 J_0 ka\left[kah_1^{(2)}(ka) \right]'
\end{aligned} \tag{21}
$$

where

$$
\left[kaj_1(ka) \right]' = \frac{d}{d(kr)}\left[krj_1(kr) \right]\big|_{r=a} \tag{22}
$$

$$
\left[kah_1^{(2)}(ka) \right]' = \frac{d}{d(kr)}\left[krh_1^{(2)}(kr) \right]\big|_{r=a} \tag{23}
$$

The total fields inside and outside the sphere are summarized as

$$
\begin{aligned}
\mathbf{E}(r,\theta,\phi) &= -j\eta_0 J_0 ka\left[kaj_1(ka) \right]' \mathbf{N}_{01}^{(4)}(r,\theta,\phi) \\
\mathbf{H}(r,\theta,\phi) &= J_0 ka\left[kaj_1(ka) \right]' \mathbf{M}_{01}^{(4)}(r,\theta,\phi) \qquad r > a
\end{aligned} \tag{24}
$$

and

$$
\begin{aligned}
\mathbf{E}(r,\theta,\phi) &= -j\eta_0 J_0 ka\left[kah_1^{(2)}(ka) \right]' \mathbf{N}_{01}^{(1)}(r,\theta,\phi) \\
\mathbf{H}(r,\theta,\phi) &= J_0 ka\left[kah_1^{(2)}(ka) \right]' \mathbf{M}_{01}^{(1)}(r,\theta,\phi) \qquad r < a
\end{aligned} \tag{25}
$$

The form of the external fields in (24) indicates that the given surface current distributed over the spherical surface generates the same field created by a *z*-directed Hertzian dipole at the coordinate origin having an appropriate dipole moment. This observation is

important in identifying the propagating- or standing-wave behavior of fields at different locations when a conducting ground plane is introduced in Chapter 3.

2.2 Radiation Quality Factor of a TM_{01}-Mode Spherical Current

For an antenna, the radiation quality factor is defined by [2]

$$Q=\begin{cases}\dfrac{2\omega W_e}{P} & W_e > W_m \\ \dfrac{2\omega W_m}{P} & W_m > W_e\end{cases} \tag{26}$$

where W_e is the time-average, non-propagating, stored electric energy, W_m is the time-average, non-propagating, stored magnetic energy, ω denotes the radian frequency, and P denotes the radiated power.

In Chu's theory, the stored energy inside the sphere was not included. The stored energy outside the sphere can be computed as

$$W_e^{r>a}=\frac{\varepsilon}{4}\iiint_V w_e dV=\frac{2\pi\varepsilon}{3k^3}\left|-J_0\eta(ka)\left[kaj_1(ka)\right]'\right|^2\left[\frac{1}{ka}+\frac{1}{(ka)^3}\right] \tag{27}$$

$$W_m^{r>a}=\frac{\mu}{4}\iiint_V w_m dV=\frac{4\pi\mu}{3k^3}\left|-J_0\eta(ka)\left[kaj_1(ka)\right]'\right|^2\frac{1}{ka} \tag{28}$$

where $W_e^{r>a}$ and $W_m^{r>a}$ are the stored energies in the $r>a$ region, $w_e=\frac{\varepsilon}{2}\left(|\mathbf{E}|^2-|\mathbf{E}_{rad}|^2\right)$ and $w_m=\frac{\mu}{2}\left(|\mathbf{H}|^2-|\mathbf{H}_{rad}|^2\right)$, here w_e and w_m represent energy densities. $\mathbf{E}_{rad}$ and $\mathbf{H}_{rad}$ are fields associated with radiation. The radiated power can be computed as

$$P_{rad} = \mathrm{Re}\left(\frac{1}{2} \oint_S \mathbf{E} \times \mathbf{H}^* \big|_{r=a} \cdot d\mathbf{S} \right) = \frac{1}{2k^2\eta} \frac{8\pi}{3} \left| -J_0\eta\left(ka\right)\left[kaj_1\left(ka\right) \right]' \right|^2 . \tag{29}$$

Choose $Q = \frac{2\omega W_e}{P}$ due to $W_e > W_m$. Finally, Chu's quality factor is

$$Q_{fs}^{Chu} = \frac{2\omega W_e^{r>a}}{P} = \frac{1}{ka} + \frac{1}{\left(ka\right)^3} . \tag{30}$$

In [6], the stored energy inside the sphere was included. This approach is closer to reality for practical antennas with air core. The electrical energy inside the sphere is added to Chu's theory. The electric energy is stored inside the sphere

$$\begin{aligned} & W_e^{r<a} \\ & = \iiint_V \frac{\varepsilon}{4} \mathbf{E} \bullet \mathbf{E}^* dV \\ & = \frac{2\pi\varepsilon}{9} \frac{\left(ka\right)^3}{2k^3} \left| -J_0\eta\left(ka\right)\left[kah_1^{(2)}\left(ka\right) \right]' \right|^2 \\ & \qquad \times \left\{ 2\left[j_0^2\left(ka\right) - j_1\left(ka\right) j_{-1}\left(ka\right) \right] + \left[j_2^2\left(ka\right) - j_1\left(ka\right) j_3\left(ka\right) \right] \right\}. \end{aligned} \tag{31}$$

Using the same approach above, quality factor inside sphere is given by

$$\begin{aligned} & Q_{r<a} \\ & = \frac{\left(ka\right)^3}{6} \frac{\left| -J_0\eta\left(ka\right)\left[kah_1^{(2)}\left(ka\right) \right]' \right|^2 \left\{ 2\left[j_0^2\left(ka\right) - j_1\left(ka\right) j_{-1}\left(ka\right) \right] + \left[j_2^2\left(ka\right) - j_1\left(ka\right) j_3\left(ka\right) \right] \right\}}{\left| -J_0\eta\left(ka\right)\left[kaj_1\left(ka\right) \right]' \right|^2} . \end{aligned} \tag{32}$$

The new quality factor is the sum of the quality factor from Chu's work and the quality factor inside the sphere. It is

$$
\begin{aligned}
Q_{fs}^{Thal} &= Q_{fs}^{Chu} + Q_{fs}^{r<a} \\
&= \frac{1}{ka} + \frac{1}{(ka)^3} \\
&+ \frac{(ka)^3}{6} \frac{\left| -J_0\eta(ka)\left[kah_1^{(2)}(ka) \right]' \right|^2 \left\{ 2\left[j_0^2(ka) - j_1(ka) j_{-1}(ka) \right] + \left[j_2^2(ka) - j_1(ka) j_3(ka) \right] \right\}}{\left| -J_0\eta(ka)\left[kaj_1(ka) \right]' \right|^2}.
\end{aligned}
\tag{33}
$$

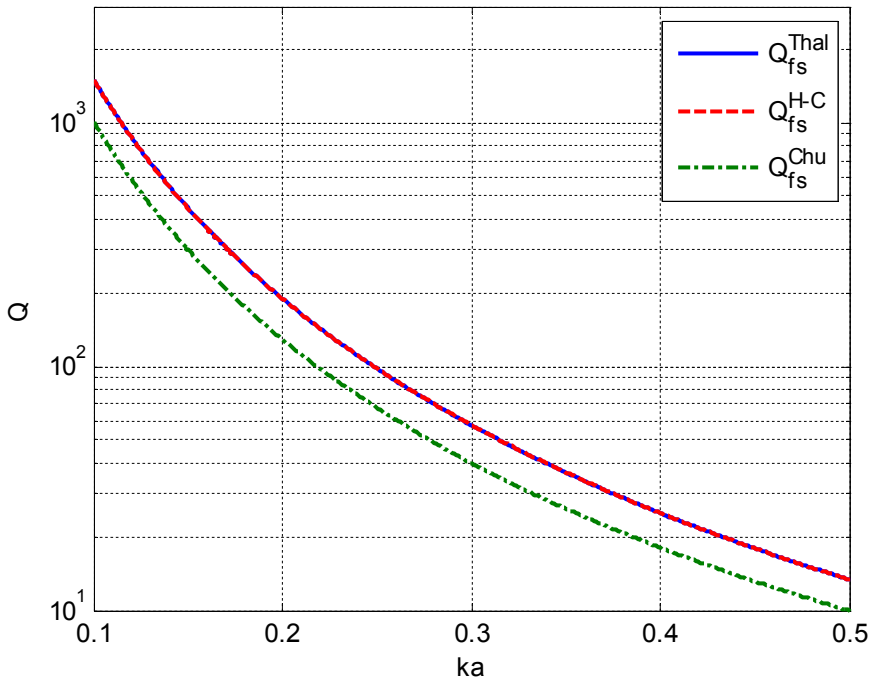

Figure 2: Comparison of three quality factors for a spherical antenna in free space.

Figure 2 compares Q_{fs}^{Chu} and Q_{fs}^{Thal} together with the approximate expression $Q_{fs}^{H\text{-}C}$ from (3). It is observed that the Q_{fs}^{Thal} curve lies on top of $Q_{fs}^{H\text{-}C}$, which validates (33).

CHAPTER 3

RADIATION QUALITY FACTOR OF A CONDUCTOR-BACKED SMALL ANTENNA

3.1 A Conductor-Backed Small Antenna

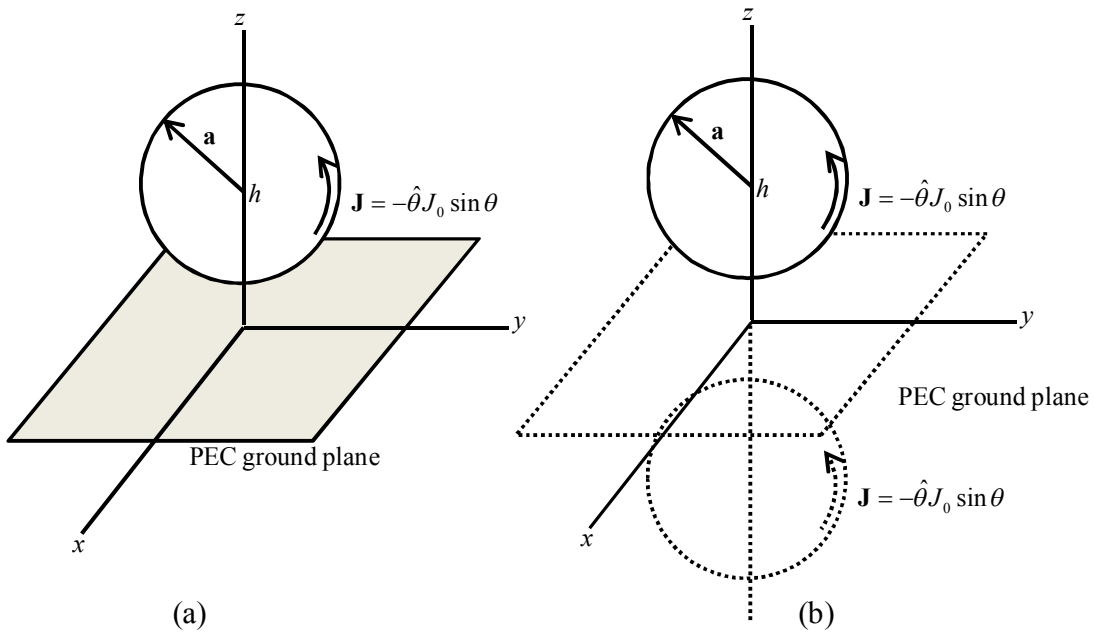

Figure 3: The problem geometry of a vertically polarized spherical antenna over a ground plane. (a) Spherical antenna above PEC ground plane. (b) After applying image theorem to replace the PEC ground plane.

In practice, an antenna is often placed above a conducting ground plane, as illustrated in Figure 3(a). In the presence of a ground plane of finite or infinite extent, part or all of the ground plane is sometimes considered to be part of the overall antenna. In the following

development, the term antenna refers to the spherical radiating structure only, without any part of the ground plane included. Furthermore, the energy stored inside the antenna refers to the non-propagating stored energy inside the spherical volume. It will be the differentiating quantity between Chu's and Thal's quality factors for the antenna in Figure 3(a) as in the free-space case of Chapter 2. The presence of a ground plane has a significant impact on the antenna quality factor. Sten *et al.* [10] used a vertical and a horizontal point dipole to compute the quality factor. However, after applying the image theory, they considered a spherical surface that circumscribes both the antenna and its image in their computation of Q. This lowers the Q value below what is physically achievable, making the minimum Q too conservative. To describe the underlying physics more accurately, the energy inside the sphere should be taken into account. From Chapter 2, the current flowing on the surface is the fundamental mode when the antenna is electrically small. Moreover, when the quality factor is significantly larger than one, the bandwidth of the antenna is approximate reciprocal of the quality factor. Currently, researchers concentrate on the fundamental mode and how to design physical antennas that closely approach the Chu bound.

To obtain the quality factor of a spherical antenna above a PEC ground plane accurately, all energy stored in fields and the radiated power should be computed. To compute the

energy, field expressions should be found first and the spherical vector wave functions are the best suited for this purpose. The **M** and **N** vectors [11], [12] work only when the antenna is placed in an unbounded, homogeneous medium. To remove the PEC ground plane, image theory is applied. According to image theory, an image antenna should be placed below the PEC ground plane when the ground plane is removed. The system, e.g. an electrically small antenna above the ground plane with ground separation h, becomes two spherical antennas separated by a center-to-center distance $2h$, as shown in Figure 3(b). Then, the vector addition theorem in spherical coordinates is applied to obtain fields centered at the coordinate origin O in the next step. After the field expressions are obtained, the stored energy can be computed by performing a volume integral of non-propagating energy densities. However, as Figure 3(b) shows, the coordinate origin is not at the center of the sphere. It is not easy to perform the volume integration if the origin is not at the center of the sphere and the shape of the volume does not coincide with constant coordinate surfaces. To overcome this difficulty, the volume integration is broken into four parts. In a regular volume region, a volume integration can be obtained in a closed form. In an irregular volume region, a volume integration can be computed numerically. The total radiated power from the two spherical antennas can be easily computed by using the known form from [13]. Once the stored energy and the radiated

power are both obtained, the radiation quality factor can be computed.

An antenna having a large effective volume has a small quality factor, associated with a broad bandwidth. According to the image theory, placing a spherical antenna above a PEC ground plane makes the effective volume larger. Hence, it is possible that the quality factor may be reduced from its free-space value after a PEC ground plane is placed. In this study, the change of the quality factor, stored energy, and radiated power will be quantified with the introduction of a ground plane. The radiation quality factor, stored energy, and radiated power in free space will be compared with the corresponding values of the antenna of the same size above a PEC ground plane. The behavior of the quality factor with respect to the antenna size ka in the range $ka<0.5$ and the ground separation kh will be investigated.

3.2 Vector Addition Theorem

When electromagnetic waves interact with spherical bodies, it is desirable in many problems to express the fields in terms of spherical vector wave functions. If a problem involves multiple electromagnetic waves due to multiple sources, it is not easy to analyze the problem in mixed coordinates. To solve a multiple sources problem, it is easier to expand those waves with respect to a common origin. As shown in Chapter 2, magnetic

and electrical fields due to a spherical antenna are well established. To move the origin away from the center of the sphere , a vector addition theorem is needed. Such an addition theorem has been reported by Cruzan [14].

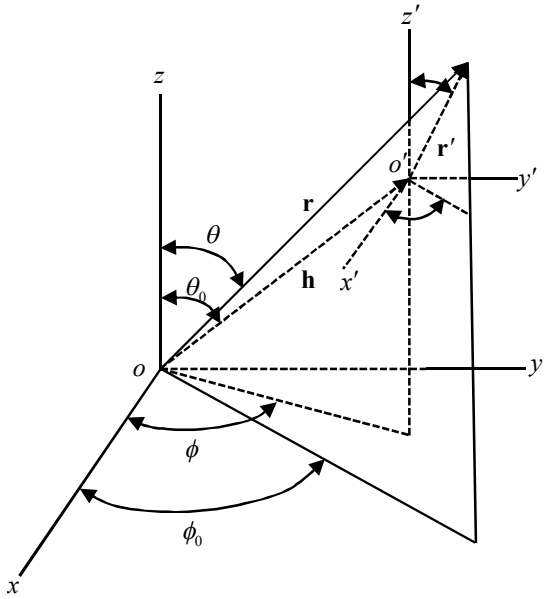

Figure 4: Translation of the coordinate origin from O to O'.

A translation of the coordinate origin from O to O' is illustrated in Figure 4. The translation vector is **h**. The spherical (r,θ,ϕ) coordinates are with respect to O and the spherical coordinates (r',θ',ϕ') are with respect to O'. The TM_{01}-mode vector spherical harmonics, $\mathbf{M}_{01}(r,\theta,\phi)$ and $\mathbf{N}_{01}(r,\theta,\phi)$, which are defined in (13) and (14), can be translated to the O' coordinate system as

$$\mathbf{M}_{01} = \sum_{v=1}^{\infty} \sum_{u=-v}^{v} \left(A_{uv}^{01} \mathbf{M}'_{uv} + B_{uv}^{01} \mathbf{N}'_{uv} \right) \tag{34}$$

$$\mathbf{N}_{01}=\sum_{v=1}^{\infty}\sum_{u=-v}^{v}\left(A_{uv}^{01}\mathbf{N}'_{uv}+B_{uv}^{01}\mathbf{M}'_{uv}\right) \tag{35}$$

where

$$A_{uv}^{01}=(-1)^{u}\sum_{p}a\left(0,1\middle|-u,v\middle|p\right)a(1,v,p)z_{p}(kh)P_{p}^{-u}(\cos\theta_{0})e^{-ju\phi_{0}} \tag{36}$$

$$B_{uv}^{01}=(-1)^{u}\sum_{p}a\left(0,1\middle|-u,v\middle|p,p-1\right)b(1,v,p)z_{p}(kh)P_{p}^{-u}(\cos\theta_{0})e^{-ju\phi_{0}}. \tag{37}$$

Note that the index v starts from one rather than zero [15]. This is due to the $(u,v)=(0,0)$ mode not corresponding to a valid solution. Here,

$$a\left(0,1\middle|-u,v\middle|p\right)=(-1)^{-u}(2p+1)\left[\frac{(v-u)!(p+u)!}{(v+u)!(p-u)!}\right]^{1/2}\begin{pmatrix}1 & v & p\\ 0 & 0 & 0\end{pmatrix}\begin{pmatrix}1 & v & p\\ 0 & 0 & 0\end{pmatrix} \tag{38}$$

$$a\left(0,1\middle|-u,v\middle|p,p-1\right)=(-1)^{-u}(2p+1)\left[\frac{(v-u)!(p+u)!}{(v+u)!(p-u)!}\right]^{1/2}\begin{pmatrix}1 & v & p\\ 0 & -u & u\end{pmatrix}\begin{pmatrix}1 & v & p\\ 0 & 0 & 0\end{pmatrix} \tag{39}$$

$$\begin{aligned}&a(1,v,p)\\&=j^{v+p-1}\left[2v(v+1)(2v+1)+(v+1)(2-v+p)(1+v-p)\right.\\&\qquad\left.-v(v+p)(3+v+p)\right]\Big/\left[2v(v+1)\right]\end{aligned} \tag{40}$$

$$\begin{aligned}&b(1,v,p)\\&=j^{v+p-1}\left[(2+v+p)(v+p-1)(1-v+p)(2+v-p)\right]^{1/2}(2v+1)\Big/\left[2v(v+1)\right]\end{aligned} \tag{41}$$

where $\begin{pmatrix}1 & v & p\\ 0 & -u & u\end{pmatrix}$ and $\begin{pmatrix}1 & v & p\\ 0 & 0 & 0\end{pmatrix}$ are the Wigner 3-j symbol [14].

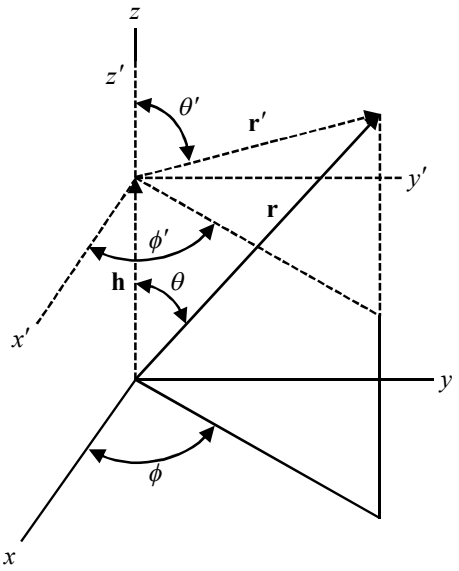

Figure 5: Translation of the coordinate system along the z axis.

Assume the translation is along the z axis. Figure 5 shows a case for θ_0=0. Then,

$P_p^u(cos\theta_0)= P_p^u(1)\neq 0$ only when u=0 and $P_p^u(1)=P_p(1)=1$ if u=0. Therefore, $\mathbf{M}_{01}(r,\theta,\phi)$ and $\mathbf{N}_{01}(r,\theta,\phi)$ can be reduced to

$$\mathbf{M}_{01}=\sum_{v=1}^{\infty}\sum_{u=-v}^{v}\left(A_{uv}^{01}\mathbf{M}'_{uv}+B_{uv}^{01}\mathbf{N}'_{uv}\right)=\sum_{v=1}^{\infty}\left(A_{0v,lower}^{01}\mathbf{M}'_{0v}+B_{0v,lower}^{01}\mathbf{N}'_{0v}\right) \tag{42}$$

$$\mathbf{N}_{01}=\sum_{v=1}^{\infty}\sum_{u=-v}^{v}\left(A_{uv}^{01}\mathbf{N}'_{uv}+B_{uv}^{01}\mathbf{M}'_{uv}\right)=\sum_{v=1}^{\infty}\left(A_{0v,lower}^{01}\mathbf{N}'_{0v}+B_{0v,lower}^{01}\mathbf{M}'_{0v}\right) \tag{43}$$

where

$$\begin{aligned}A_{0v,lower}^{01}&=\sum_{p}a\left(0,1\middle|0,v\middle|p\right)a\left(1,v,p\right)z_p\left(kh\right)\\&=\sum_{p}\left(2p+1\right)\begin{pmatrix}1&v&p\\0&0&0\end{pmatrix}\begin{pmatrix}1&v&p\\0&0&0\end{pmatrix}\\&\quad\times j^{v+p-1}\left[2v\left(v+1\right)\left(2v+1\right)+\left(v+1\right)\left(2-v+p\right)\left(1+v-p\right)\right.\\&\qquad\left.-v\left(v+p\right)\left(3+v+p\right)\right]/\left[2v\left(v+1\right)\right]z_p\left(kh\right)\end{aligned} \tag{44}$$

$$A_{0v,lower}^{01} = \sum_p a\left(0,1\middle|0,v\middle|p\right)a\left(1,v,p\right)z_p\left(kh\right)$$
$$= \sum_p \left(2p+1\right)\begin{pmatrix}1 & v & p\\ 0 & 0 & 0\end{pmatrix}\begin{pmatrix}1 & v & p\\ 0 & 0 & 0\end{pmatrix} \qquad (45)$$
$$\times j^{v+p-1}\left[2v\left(v+1\right)\left(2v+1\right)+\left(v+1\right)\left(2-v+p\right)\left(1+v-p\right)\right.$$
$$\left.-v\left(v+p\right)\left(3+v+p\right)\right]/\left[2v\left(v+1\right)\right]z_p\left(kh\right)$$

The coefficient, $B_{0v,lower}^{01}$, is equal to zero for the TM_{01} mode.

In the addition theorem, the field expression outside a sphere is divided into two regions [14], $r'>h$ and $r'<h$.

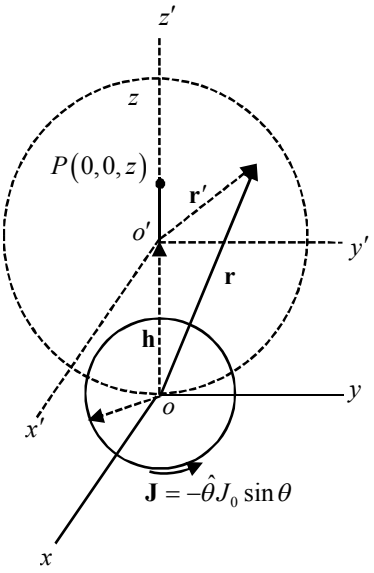

Figure 6: Fields expanded by O' inside the boundary.

In $r'<h$, as shown Figure 6, the $\mathbf{M}_{0v}(r',\theta',\phi')$ and $\mathbf{N}_{0v}(r',\theta',\phi')$ functions are

$$\mathbf{M}_{0v}\left(r',\theta',\phi'\right) = \mathbf{M}_{0v}^{(1)}\left(r',\theta',\phi'\right) = -\hat{\phi}' j_v\left(kr'\right)P_v^1\left(\cos\theta'\right) \qquad (46)$$

$$\begin{aligned}\mathbf{N}_{0v}\left(r',\theta',\phi'\right)&=\mathbf{N}_{0v}^{(1)}\left(r',\theta',\phi'\right)\\&=\hat{r}'\frac{v\left(v+1\right)}{kr'}j_v\left(kr'\right)P_v\left(\cos\theta'\right)+\hat{\theta}'\left[j_{v-1}\left(kr'\right)-v\frac{j_v\left(kr'\right)}{kr'}\right]P_v^1\left(\cos\theta'\right).\end{aligned}\tag{47}$$

In $r'<h$, $h_p^{(2)}(kh)$ is chosen for $z_p(kh)$. In addition, $\mathbf{M}_{01}^{(4)}(r,\theta,\phi)$ and $\mathbf{N}_{01}^{(4)}(r,\theta,\phi)$ in this region can be expanded in terms of $\mathbf{M}_{0v}^{(1)}(r',\theta',\phi')$ and $\mathbf{N}_{0v}^{(1)}(r',\theta',\phi')$ as

$$\begin{aligned}\mathbf{M}_{01}^{(4)}\left(r,\theta,\phi\right)&=\sum_{v=1}^{\infty}A_{0v,lower}^{01}\mathbf{M}_{0v}^{(1)}\left(r',\theta',\phi'\right)\\\mathbf{N}_{01}^{(4)}\left(r,\theta,\phi\right)&=\sum_{v=1}^{\infty}A_{0v,lower}^{01}\mathbf{N}_{0v}^{(1)}\left(r',\theta',\phi'\right).\end{aligned}\tag{48}$$

Using (47), the electric and magnetic fields due to the spherical current centered at O are represented by

$$\begin{aligned}\mathbf{E}\left(r,\theta,\phi\right)&=a_{01}\mathbf{M}_{01}^{(4)}\left(r,\theta,\phi\right)+b_{01}\mathbf{N}_{01}^{(4)}\left(r,\theta,\phi\right)\\&=a_{01}\sum_{v=1}^{\infty}A_{0v,lower}^{01}\mathbf{M}_{0v}^{(1)}\left(r',\theta',\phi'\right)+b_{01}\sum_{v=1}^{\infty}A_{0v,lower}^{01}\mathbf{N}_{0v}^{(1)}\left(r',\theta',\phi'\right)\\&=-j\eta_0J_0ka\left[kaj_1\left(ka\right)\right]'\sum_{v=1}^{\infty}A_{0v,lower}^{01}\mathbf{N}_{0v}^{(1)}\left(r',\theta',\phi'\right)\\&=\alpha_E^{out}\sum_{v=1}^{\infty}A_{0v,lower}^{01}\mathbf{N}_{0v}^{(1)}\left(r',\theta',\phi'\right)\end{aligned}\tag{49}$$

$$\begin{aligned}\mathbf{H}\left(r,\theta,\phi\right)&=\frac{jk}{\eta_0}\left[a_{01}\mathbf{N}_{01}^{(4)}\left(r,\theta,\phi\right)+b_{01}\mathbf{M}_{01}^{(4)}\left(r,\theta,\phi\right)\right]\\&=\frac{jk}{\eta_0}\left\{a_{01}\sum_{v=1}^{\infty}A_{0v,lower}^{01}\mathbf{N}_{0v}^{(1)}\left(r',\theta',\phi'\right)+b_{01}\sum_{v=1}^{\infty}A_{0v,lower}^{01}\mathbf{M}_{0v}^{(1)}\left(r',\theta',\phi'\right)\right\}\\&=J_0ka\left[kaj_1\left(ka\right)\right]'\sum_{v=1}^{\infty}A_{0v,lower}^{01}\mathbf{M}_{0v}^{(1)}\left(r',\theta',\phi'\right)\\&=\alpha_H^{out}\sum_{v=1}^{\infty}A_{0v,lower}^{01}\mathbf{M}_{0v}^{(1)}\left(r',\theta',\phi'\right)\end{aligned}\tag{50}$$

where

$$\alpha_E^{out}=-j\eta_0J_0ka\left[kaj_1\left(ka\right)\right]'\tag{51}$$

$$\alpha_H^{out} = J_0 ka\left[kaj_1(ka)\right]'. \tag{52}$$

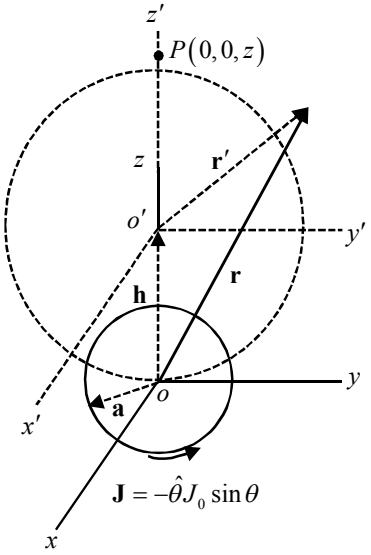

Figure 7: Fields expanded by O' outside the boundary.

In $r'>h$, as shown Figure 7, the $\mathbf{M}_{0v}(r',\theta',\phi')$ and $\mathbf{N}_{0v}(r',\theta',\phi')$ functions are

$$\mathbf{M}_{0v}(r',\theta',\phi') = \mathbf{M}_{0v}^{(4)}(r',\theta',\phi') = -\hat{\phi}' h_v^{(2)}(kr') P_v^1(\cos\theta') \tag{53}$$

$$\begin{aligned}\mathbf{N}_{0v}(r',\theta',\phi') &= \mathbf{N}_{0v}^{(4)}(r',\theta',\phi') \\ &= \hat{r}' \frac{v(v+1)}{kr'} h_v^{(2)}(kr') P_v(\cos\theta') + \hat{\theta}' \left[h_{v-1}^{(2)}(kr') - v\frac{h_v^{(2)}(kr')}{kr} \right] P_v^1(\cos\theta')\end{aligned} \tag{54}$$

In $r'>h$, $j_p(kh)$ is chosen for $z_p(kh)$. In addition, $\mathbf{M}_{01}^{(4)}(r,\theta,\phi)$ and $\mathbf{N}_{01}^{(4)}(r,\theta,\phi)$ in this region can be expanded by $\mathbf{M}_{0v}^{(4)}(r',\theta',\phi')$ and $\mathbf{N}_{0v}^{(4)}(r',\theta',\phi')$ as

$$\begin{aligned}\mathbf{M}_{01}^{(4)}(r,\theta,\phi) &= \sum_{v=1}^{\infty} A_{0v,lower}^{01} \mathbf{M}_{0v}^{(4)}(r',\theta',\phi') \\ \mathbf{N}_{01}^{(4)}(r,\theta,\phi) &= \sum_{v=1}^{\infty} A_{0v,lower}^{01} \mathbf{N}_{0v}^{(4)}(r',\theta',\phi')\end{aligned} \tag{55}$$

The fields in this region are represented by

$$
\begin{aligned}
&\mathbf{E}(r,\theta,\phi) = a_{01}\mathbf{M}_{01}^{(4)}(r,\theta,\phi) + b_{01}\mathbf{N}_{01}^{(4)}(r,\theta,\phi) \\
&= a_{01}\sum_{v=1}^{\infty} A_{0v,lower}^{01}\mathbf{M}_{0v}^{(4)}(r',\theta',\phi') + b_{01}\sum_{v=1}^{\infty} A_{0v,lower}^{01}\mathbf{N}_{0v}^{(4)}(r',\theta',\phi') \\
&= -j\eta_0 J_0 ka\left[kaj_1(ka)\right]'\sum_{v=1}^{\infty} A_{0v,lower}^{01}\mathbf{N}_{0v}^{(4)}(r',\theta',\phi') \\
&= \alpha_E^{out}\sum_{v=1}^{\infty} A_{0v,lower}^{01}\mathbf{N}_{0v}^{(4)}(r',\theta',\phi')
\end{aligned}
\tag{56}
$$

$$
\begin{aligned}
&\mathbf{H}(r,\theta,\phi) = \frac{jk}{\eta_0}\left[a_{01}\mathbf{N}_{01}^{(4)}(r,\theta,\phi) + b_{01}\mathbf{M}_{01}^{(4)}(r,\theta,\phi)\right] \\
&= \frac{jk}{\eta_0}\left\{a_{01}\sum_{v=1}^{\infty} A_{0v,lower}^{01}\mathbf{N}_{0v}^{(4)}(r',\theta',\phi') + b_{01}\sum_{v=1}^{\infty} A_{0v,lower}^{01}\mathbf{M}_{0v}^{(4)}(r',\theta',\phi')\right\} \\
&= J_0 ka\left[kaj_1(ka)\right]'\sum_{v=1}^{\infty} A_{0v,lower}^{01}\mathbf{M}_{0v}^{(4)}(r',\theta',\phi') \\
&= \alpha_H^{out}\sum_{v=1}^{\infty} A_{0v,lower}^{01}\mathbf{M}_{0v}^{(4)}(r',\theta',\phi')
\end{aligned}
\tag{57}
$$

Following the same method above, it is easy to obtain the field expressions for $\theta_0=\pi$.

There, only coefficient is different. Specifically, the coefficient $A_{0v,upper}^{01}$ is changed to

$$
\begin{aligned}
A_{0v,upper}^{01} &= \sum_p (-1)^p\, a(0,1|0,v|p)\, a(1,v,p)\, z_p(kh) \\
&= \sum_p (-1)^p (2p+1)\begin{pmatrix} 1 & v & p \\ 0 & 0 & 0 \end{pmatrix}\begin{pmatrix} 1 & v & p \\ 0 & 0 & 0 \end{pmatrix} \\
&\quad \times j^{v+p-1}\left[2v(v+1)(2v+1) + (v+1)(2-v+p)(1+v-p)\right. \\
&\qquad \left. - v(v+p)(3+v+p)\right] / \left[2v(v+1)\right] z_p(kh)
\end{aligned}
\tag{58}
$$

3.3 Non-Propagating Stored Energy

3.3.1 Division of Space and *Q*-Computation Approach

The original problem is to investigate the quality factor for a spherical antenna above a PEC ground plane, shown in Figure 3(a). The analysis method for free-space antennas cannot be directly applied due to a planar boundary of the ground plane. To remove the PEC ground plane, the image theory is applied. According to the image theory, a spherical image antenna should be place below the PEC ground plane. The distance between the ground plane and the image antenna is equal to the distance between the ground plane and the original antenna. After this process, the configuration in Figure 3(b) results. This is a two-spherical-antenna system in free space. Using the addition theorem, the fields due to original and image spherical antennas can be expanded in the (x,y,z) coordinate system having the original ground plane in x-y plane. By applying this method, the fields from both antennas are represented in the same coordinate system using a common set of vector expansion functions.

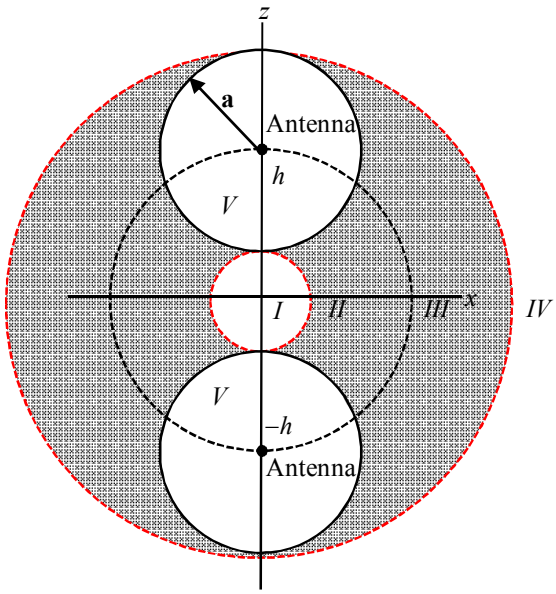

Figure 8: Boundaries for the addition theorem and volume integrations.

The fields from this two-antenna system are known everywhere. Therefore, the stored energy can be computed by performing a volume integration over a proper volume, which is all space extending to infinity. Since only the non-propagating energy should be taken into account when computing the radiation Q, different regions of space need to be identified depending on the presence or absence of energy associated with radiation. The result of this identification is the five distinct regions illustrated in Figure 8. In Chapter 2, it has been identified that the prescribed surface current excites only the fundamental TM_{01} mode outside the sphere. In other words, for field points outside the spherical antenna surface, the surface current distribution can be replaced by an equivalent

Hertzian dipole. Hence, at any observation point outside the two antenna spheres in Figure 8, the total field can be obtained by a vector sum of fields generated by two equivalent Hertzian dipoles located at the two sphere centers $(x,y,z)=(0,0,h)$ and $(0,0,-h)$. This makes the spherical surface (black dashed contour) of radius h centered at the coordinate origin the boundary between two volumes having standing-wave (inside) and propagating-wave (outside) characteristics. Inside this boundary (regions I and II), Bessel function of the first kind is the radial function and Hankel function of the second kind is in the expansion coefficients. Outside this boundary (regions III and IV), Hankel function of the second kind is the radial function and Bessel function of the first kind is in the coefficients.

The red dashed circles are the boundaries for volume integrations. Inside the small red dashed circle (region I) and outside the large red dashed circle (region IV), volume integrations can be obtained in closed form as an infinite series. The non-propagating stored electric and magnetic energies are

$$W_e = \iiint_V w_e dV,\ w_e = \frac{\varepsilon}{2}\left(|\mathbf{E}|^2 - |\mathbf{E}_{rad}|^2\right) \tag{59}$$

$$W_m = \iiint_V w_m dV,\ w_m = \frac{\mu}{2}\left(|\mathbf{H}|^2 - |\mathbf{H}_{rad}|^2\right) \tag{60}$$

where w_e and w_m represent the corresponding energy densities. $\mathbf{E}_{rad}$ and $\mathbf{H}_{rad}$ are fields associated with radiation.

Inside the small red dashed circle region (region I), integration limits are from 0 to 2π for ϕ, from 0 to π for θ, and from 0 to h-a for r. Outside large the red circle region (region IV), they are from 0 to 2π for ϕ, from 0 to π for θ, and from h+a to ∞ for r. However, the volume integration for the shaded region (regions II and III) cannot be obtained in a closed form because the shape of this region is irregular. The two spherical volumes are excluded in this computation, and the integration is performed numerically.

The integration described above computes the stored energy outside the two spheres. For the stored energy inside the two spheres, we can move the coordinate origin to the center of one sphere and use the vector addition theorem to find the total field due to both antennas. Then, a volume integration over the sphere can be performed to find the energy stored inside the spherical antenna. The stored energy inside the other sphere is the same due to symmetry.

The radiated power of the two-sphere system is

$$P = \mathrm{Re}\left(\frac{1}{2} \oint_S \mathbf{E} \times \mathbf{H}^* \big|_{r=d+a} \cdot d\mathbf{S} \right). \tag{61}$$

Working the vector addition theorem above, the fields are expanded at the center of the (x,y,z) coordinate system. The radiated power P is obtained setting the closed surface S to the spherical surface represented by the large red circle Figure 8.

All needed energy is computed. According to the definition of quality vector, substitute all numbers into the definition,

$$Q = \frac{2\omega W_{e\,or\,m}}{P} \tag{62}$$

and we can obtain the quality factor for this system.

3.3.2 Region I

According to Section 3.2, the total fields can be represented by

$$\mathbf{E}(r,\theta,\phi) = \alpha_E^{out} \sum_{v=1}^{\infty} \left(A_{0v,lower}^{01} + A_{0v,upper}^{01} \right) \mathbf{N}_{0v}^{(1)}(r',\theta',\phi') = \alpha_E^{out} \sum_{v=1}^{\infty} A_{0v}^{01} \mathbf{N}_{0v}^{(1)}(r',\theta',\phi') \tag{63}$$

$$\mathbf{H}(r,\theta,\phi) = \alpha_H^{out} \sum_{v=1}^{\infty} \left(A_{0v,lower}^{01} + A_{0v,upper}^{01} \right) \mathbf{M}_{0v}^{(1)}(r',\theta',\phi') = \alpha_H^{out} \sum_{v=1}^{\infty} A_{0v}^{01} \mathbf{M}_{0v}^{(1)}(r',\theta',\phi') \tag{64}$$

where

$$A_{0v}^{01} = A_{0v,lower}^{01} + A_{0v,upper}^{01} \tag{65}$$

In region I, fields are given by (63) and (64). The radial function is the Bessel function. The electric and magnetic fields in this region are standing waves. There is no field associated with radiation to far-field region. Therefore, $\mathbf{E}_{rad}$ and $\mathbf{H}_{rad}$ in (59) and (60) are equal to zero. The non-propagating, stored electrical energy in region I is

$$W_e^I = \frac{\varepsilon}{4} \iiint_V \mathbf{E} \cdot \mathbf{E}^* dV = \frac{\varepsilon}{4} \iiint_V \left\{ \alpha_E^{out} \sum_{v=1}^{\infty} A_{0v}^{01} \mathbf{N}_{0v}^{(1)}(r,\theta,\phi) \cdot \left[\alpha_E^{out} \sum_{v=1}^{\infty} A_{0v}^{01} \mathbf{N}_{0v}^{(1)}(r,\theta,\phi) \right]^* \right\} dV \tag{66}$$

Due to the orthogonal relationship, (66) can be reduced to

$$
\begin{aligned}
W_e^I &= \frac{\varepsilon}{4}\iiint_V \mathbf{E}\cdot\mathbf{E}^* dV = \frac{\varepsilon}{4}\left(\alpha_E^{out}\right)^2 \iiint_V \left\{ \sum_{v=1}^{\infty}\left(A_{0v}^{01}\right)^2 \mathbf{N}_{0v}^{(1)}\left(r,\theta,\phi\right)\cdot\mathbf{N}_{0v}^{(1)}\left(r,\theta,\phi\right)\right\} dV \\
&= \sum_{v=1}^{\infty}\frac{\varepsilon}{4}\left(\alpha_E^{out}\right)^2 \iiint_V \left(A_{0v}^{01}\right)^2 \mathbf{N}_{0v}^{(1)}\left(r,\theta,\phi\right)\cdot\mathbf{N}_{0v}^{(1)}\left(r,\theta,\phi\right) dV \\
&= \sum_{v=1}^{\infty} W_e^v
\end{aligned}
\tag{67}
$$

where

$$
\begin{aligned}
W_e^v &= \frac{\varepsilon}{4}\left(\alpha_E^{out}\right)^2 \iiint_V \left|A_{0v}^{01}\right|^2 \mathbf{N}_{0v}^{(1)}\left(r,\theta,\phi\right)\cdot\mathbf{N}_{0v}^{(1)}\left(r,\theta,\phi\right) dV \\
&= \frac{\varepsilon}{4}\left(\alpha_E^{out}\left|A_{0v}^{01}\right|\right)^2 \frac{4\pi}{\left(2v+1\right)^2} v\left(v+1\right) \\
&\quad\times\left\{ \left(v+1\right)\frac{\pi^2}{2k^3}\frac{\left(kh-ka\right)\left[j_{v-1}^2\left(kh-ka\right) - j_v\left(kh-ka\right)J_{v-2}\left(kh-ka\right)\right]}{4}\cdot \right. \\
&\qquad \left. + v\frac{\pi^2}{2k^3}\frac{\left(kh-ka\right)\left[j_{v+1}^2\left(kh-ka\right) - j_v\left(kh-ka\right) j_{v+2}\left(kh-ka\right)\right]}{4}\right\}
\end{aligned}
\tag{68}
$$

Using the same approach, the magnetic energy is found to be

$$
\begin{aligned}
W_m^I &= \frac{\mu}{4}\iiint_V \mathbf{H}\cdot\mathbf{H}^* dV \\
&= \frac{\mu}{4}\iiint_V \left\{ \alpha_H^{out}\sum_{v=1}^{\infty} A_{0v}^{01}\mathbf{M}_{0v}^{(1)}\left(r,\theta,\phi\right)\cdot\left[\alpha_H^{out}\sum_{v=1}^{\infty} A_{0v}^{01}\mathbf{M}_{0v}^{(1)}\left(r,\theta,\phi\right)\right]^*\right\} dV \\
&= \sum_{v=1}^{\infty} W_m^v
\end{aligned}
\tag{69}
$$

where

$$
\begin{aligned}
W_m^v &= \left(\alpha_H^{out}\left|A_{0v}^{01}\right|\right)^2 \frac{4\pi}{2v+1} v\left(v+1\right)\frac{\pi^2}{2k^3} \\
&\quad\times\frac{\left(kh-ka\right)\left[j_v^2\left(kh-ka\right) - j_{v-1}\left(kh-ka\right) j_{v+1}\left(kh-ka\right)\right]}{4}\cdot
\end{aligned}
\tag{70}
$$

3.3.3 Region II

The electric and magnetic fields in region II are standing waves. There is no field associated with radiation. Hence, $\mathbf{E}_{rad}$ and $\mathbf{H}_{rad}$ in (59) and (60) are equal to zero. However, the volume in region II is not appropriate to obtain the integral in a close form. Hence, numerical integration is applied in this region and the addition theorem is not applied at this point. The fields, $\mathbf{E}(x_1,y_1,z_1)$ and $\mathbf{H}(x_1,y_1,z_1)$, can be represented in the (x_1,y_1,z_1) system having the origin is at $(x,y,z)=(0,0,-h)$. The fields, $\mathbf{E}(x_2,y_2,z_2)$ and $\mathbf{H}(x_2,y_2,z_2)$, can be represented in the (x_2,y_2,z_2) coordinate system having the origin at $(x,y,z)=(0,0,h)$.

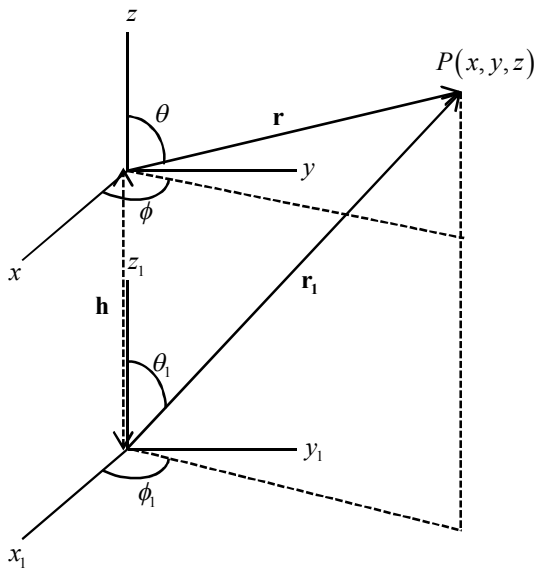

Figure 9: Two different coordinate systems (x,y,z) and (x_1,y_1,z_1) .

From Figure 9, the relationships between the spherical coordinates of the two systems are

$$r_1 = \sqrt{r^2 + 2hr\cos\theta + h^2} \tag{71}$$

$$\theta_1 = \cos^{-1}\left(\frac{r\cos\theta + h}{r_1}\right) \tag{72}$$

The fields due to the antenna for which the center is at (0,0,-*h*) are

$$\mathbf{E}(r_1,\theta_1,\phi_1) = -j\eta_0 J_0 ka\left[kaj_1(ka)\right]' \mathbf{N}_{01}^{(4)}(r_1,\theta_1,\phi_1) \tag{73}$$

$$\mathbf{H}(r_1,\theta_1,\phi_1) = J_0 ka\left[kaj_1(ka)\right]' \mathbf{M}_{01}^{(4)}(r_1,\theta_1,\phi_1) \tag{74}$$

Substituting (71) and (72) into (73) and (74), the field expression are written in the (*x,y,z*) coordinate system.

There are two antennas in the system. The fields due the antenna centered at (0,0,*h*) can be represented in the (*x,y,z*) coordinate system by repeating the same procedure.

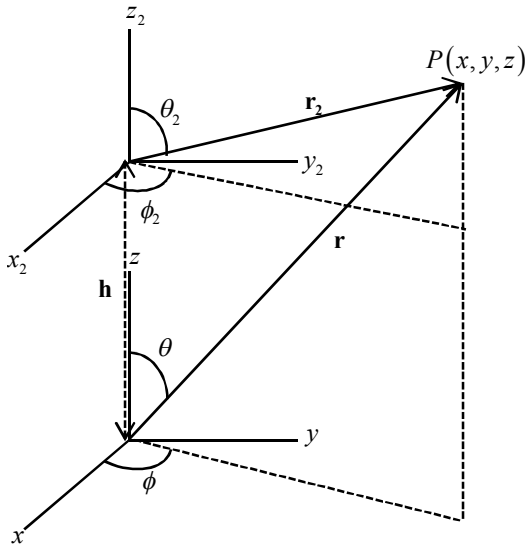

Figure 10: Two different coordinate systems (*x,y,z*) and (x_2,y_2,z_2) .

The relationships between spherical coordinates in the two systems are

$$r_2 = \sqrt{r^2 - 2hr\cos\theta + h^2} \tag{75}$$

$$\theta_2 = \cos^{-1}\left(\frac{r\cos\theta - h}{r_2}\right) \tag{46}$$

The fields due to the antenna having the center is at (0,0,h) are

$$\mathbf{E}(r_2,\theta_2,\phi_2) = -j\eta_0 J_0 ka\left[kaj_1(ka)\right]' \mathbf{N}_{01}^{(4)}(r_2,\theta_2,\phi_2) \tag{77}$$

$$\mathbf{H}(r_2,\theta_2,\phi_2) = J_0 ka\left[kaj_1(ka)\right]' \mathbf{M}_{01}^{(4)}(r_2,\theta_2,\phi_2). \tag{78}$$

Substituting (75) and (76) into (77) and (78), the field expression can be represented in the (x,y,z) coordinate system. Finally, the total fields can be represented by

$$\mathbf{E}(r,\theta,\phi) = \mathbf{E}(r_1,\theta_1,\phi_1) + \mathbf{E}(r_2,\theta_2,\phi_2) \tag{79}$$

$$\mathbf{H}(r,\theta,\phi) = \mathbf{H}(r_1,\theta_1,\phi_1) + \mathbf{H}(r_2,\theta_2,\phi_2). \tag{80}$$

The total fields due to two different antennas can be represented in the (x,y,z) coordinate system. After finding the fields everywhere in the region, the numerical volume integration is performed.

3.3.4 Region III

The electric and magnetic fields in region III are propagating waves. There is some energy associated with radiation. To compute the non-propagating stored energy, the energy associated with the radiated fields should be subtracted from total energy.

Collin and Rothschild [16] presented a simple approach to compute the stored energy. They found the difference of magnetic stored energy and electrical stored energy by integrating the complex Poynting vector over a closed surface,

$$\frac{1}{2}\oint_S \mathbf{E}\times\mathbf{H}^*\bullet d\mathbf{S} = P + 2j\omega\left(W_m - W_e\right) \tag{81}$$

where P is total radiated power.

They realized that the energy density associated with the radiation field was the real part of the radial component of the complex Poynting vector divided by the speed of energy flow. It is

$$w_e^r + w_m^r = \left(\mu_0\varepsilon_0\right)^{1/2}\,\mathrm{Re}\left(\frac{1}{2}\mathbf{E}\times\mathbf{H}^*\right) \tag{82}$$

where w_e^r is the electric energy density associated with radiation and w_m^r is the magnetic energy density associated with radiation.

The total energy density associated with radiation can be obtained from (82). To compute the total stored energy, this quantity should be subtracted from the total energy, *i.e.*

$$W_m^{III} + W_e^{III} = \iiint_V \left[\frac{\varepsilon}{4}\mathbf{E}\cdot\mathbf{E}^* + \frac{\mu}{4}\mathbf{H}\cdot\mathbf{H}^* - \left(w_e^r + w_m^r\right)\right]dV \tag{83}$$

From (81) and (83), the non-propagating, stored magnetic and electric energies can be obtained. The volume in this region is irregular. The integration cannot be obtained in closed form. In addition, numerical integration is applied in this region as the method in region II. The field expression should be represented as (79) and (80). The volume integration should be performed numerically.

3.3.5 Region IV

In region IV, field expressions are given by (62) and (63). The radial function is Hankel function of the second kind. The waves in this region are propagating waves. Some energy associated with propagating wave should be subtracted. According to [17], total non-propagating, stored energy is

$$\begin{aligned} & W_e^{IV} + W_m^{IV} \\ & = \frac{\varepsilon}{4k^3} \sum_{v=1}^{\infty} \frac{4\pi}{2v+1} v(v+1) \left| \alpha_E^{out} A_{0v}^{01} \right|^2 2kh - (kh)^3 \\ & \qquad \times \left\{ \left[\left| h_v^{(2)}(kh) \right|^2 - j_{v-1}(kh) j_{v+1}(kh) - y_{v-1}(kh) y_{v+1}(kh) \right] \right. \\ & \qquad \left. - (kh)^2 \left[j_v(kh) j_v'(kh) + y_v(kh) y_v'(kh) \right] - kh \left| h_v^{(2)}(kh) \right|^2 \right\} \end{aligned} \quad . \tag{84}$$

The difference between non-propagating, stored electrical and magnetic energy is

$$\begin{aligned} & W_e^{IV} - W_m^{IV} \\ & = \frac{\varepsilon h}{4k^2} \sum_{v=1}^{\infty} \frac{4\pi}{2v+1} v(v+1) \left(- \left| \alpha_E^{out} A_{0v}^{01} \right|^2 \right) \left\{ \left| h_v^{(2)}(kh) \right| + kh \left[j_v(kh) j_v'(kh) + y_v(kh) y_v'(kh) \right] \right\} \cdot \end{aligned} \tag{85}$$

The non-propagating, stored electric and magnetic energies can be obtained from (84) and (85).

3.3.6 Region V

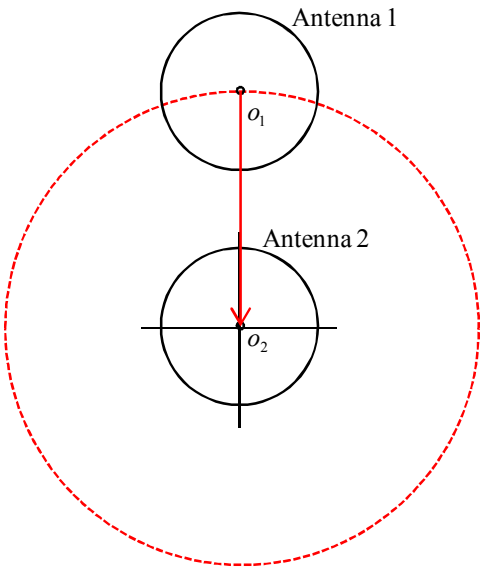

Figure 11: The translation coordinate from O_1 to O_2.

To obtain the electric and magnetic energy inside the spherical antenna, it is easy to integrate if the origin is set at the center of the one of spheres. Figure 11 shows the origin of antenna 1, O_1, is moved to the origin of antenna 2, O_2. The electric and magnetic fields due to antenna 1 can be expanded at O_2. The fields due to antenna 1 ,expanded around O_2, are

$$\mathbf{E}(r,\theta,\phi) = \alpha_E^{out,1} \sum_{v=1}^{\infty} A_{0v,lower}^{01} \mathbf{N}_{0v}^{(1)}(r,\theta,\phi) \tag{86}$$

$$\mathbf{H}(r,\theta,\phi) = \alpha_H^{out,1} \sum_{v=1}^{\infty} A_{0v,lower}^{01} \mathbf{M}_{0v}^{(1)}(r,\theta,\phi) \tag{87}$$

where

$$\alpha_E^{out,1} = -j\eta_0 J_0 ka\left[kaj_1(ka)\right]' \tag{88}$$

$$\alpha_H^{out,1} = J_0 ka\left[kaj_1(ka)\right]'. \tag{89}$$

The fields due to antenna 2, expanded around O_2, are

$$\mathbf{E}(r,\theta,\phi) = \alpha_E^{in,2} \mathbf{N}_{01}^{(1)}(r,\theta,\phi) \tag{90}$$

$$\mathbf{H}(r,\theta,\phi) = \alpha_H^{in,2} \mathbf{M}_{01}^{(1)}(r,\theta,\phi) \tag{91}$$

where

$$\alpha_E^{in,2} = -j\eta_0 J_0 ka\left[kah_1^{(2)}(ka)\right]' \tag{92}$$

$$\alpha_H^{in,2} = J_0 ka\left[kah_1^{(2)}(ka)\right]'. \tag{93}$$

Finally, the total fields are

$$\mathbf{E} = \sum_{v=1}^{\infty} \left(\alpha_E^{out,1} A_{0v}^{01} + \delta_{1v}\alpha_E^{in,2}\right) \mathbf{N}_{0v}^{(1)}(r,\theta,\phi) \tag{94}$$

$$\mathbf{H} = \sum_{v=1}^{\infty} \left(\alpha_H^{out,1} A_{0v}^{01} + \delta_{1v}\alpha_H^{in,2}\right) \mathbf{M}_{0v}^{(1)}(r,\theta,\phi) \tag{95}$$

where δ_{1v}=1 when v=1 and δ_{1v}=1 otherwise.

In region V, there is no field associated with radiation. Hence, $\mathbf{E}_{rad}$ and $\mathbf{H}_{rad}$ in (59) and (60) are equal to zero. The electric and magnetic energies are equal to

$$
\begin{aligned}
W_e^V &= \frac{\varepsilon}{4}\iiint_V \mathbf{E}\cdot\mathbf{E}^* dV \\
&= \frac{\varepsilon}{4}\sum_{v=1}^{\infty}\left|\alpha_E^{out,1}A_{0v}^{01}+\delta_{1v}\alpha_E^{in,2}\right|^2 \frac{4\pi}{(2v+1)^2}v(v+1) \\
&\quad\times\left\{(v+1)\frac{(ka)^3}{2k^3}\left[j_{v-1}^2(ka)-j_v(ka)\,j_{v-2}(ka)\right]+v\frac{(ka)^3}{2k^3}\left[j_{v+1}^2(ka)-j_v(ka)\,j_{v+2}(ka)\right]\right\}
\end{aligned} \tag{96}
$$

$$
\begin{aligned}
W_m^V &= \frac{\mu}{4}\iiint_V \mathbf{H}\cdot\mathbf{H}^* dV \\
&= \frac{\mu}{4}\sum_{v=1}^{\infty}\left|\alpha_H^{out,1}A_{0v}^{01}+\delta_{1v}\alpha_H^{in,2}\right|^2 \frac{4\pi}{2v+1}v(v+1)\frac{(ka)^3}{2k^3}\left[j_v^2(ka)-j_{v-1}(ka)\,j_{v+1}(ka)\right]
\end{aligned} . \tag{97}
$$

3.3.7 Radiated Power

The field expressions in region IV are

$$
\mathbf{E}(r,\theta,\phi) = \alpha_E^{out}\sum_{v=1}^{\infty}A_{0v}^{01}\mathbf{N}_{0v}^{(4)} = \alpha_E^{out}\sum_{v=1}^{\infty}A_{0v}^{01}\mathbf{N}_{0v}^{(4)} \tag{98}
$$

$$
\mathbf{H}(r,\theta,\phi) = \alpha_H^{out}\sum_{v=1}^{\infty}A_{0v}^{01}\mathbf{M}_{0v}^{(4)} = \alpha_H^{out}\sum_{v=1}^{\infty}A_{0v}^{01}\mathbf{M}_{0v}^{(4)} \tag{99}
$$

According to [13], radiated power is represented

$$
P_v^{TM} = \frac{\left|\alpha_E^{out}\right|^2}{2k^2\eta}\lambda_{0v}\left|A_{0v}^{01}\right|^2 \tag{100}
$$

where

$$
\lambda_{0v} = v(v+1)\frac{4\pi}{2v+1}. \tag{101}
$$

In addition, the total radiated power is

$$
P^{TM} = \sum_{v=1}^{\infty}\frac{\left|\alpha_E^{out}\right|^2}{2k^2\eta}\lambda_{0v}\left|A_{0v}^{01}\right|^2. \tag{102}
$$

CHAPTER 4

THEORETICAL RESULTS

Following the procedure described in Section 3.3, all the energy and power quantities needed for the quality factor can be computed. Now, several quantities are defined for different quality factors. Q_{fs}^{Chu} is defined by Chu's quality factor in free space. This quality factor excludes the stored energy inside the radius a and the antenna is placed in free space. Q_{fs}^{Thal} is defined by Thal's quality factor. This quality factor includes the stored energy inside the spherical surface of radius a and the antenna is placed in free space. Q_{gnd}^{Chu} is defined by Chu's definition of quality factor but the antenna is placed above a PEC ground plane. This quality factor excludes the energy inside the spherical antenna. Q_{gnd}^{Thal} is defined by Thal's definition of quality factor but the antenna is placed above a PEC ground plane. This quality factor includes the energy inside the spherical antenna.

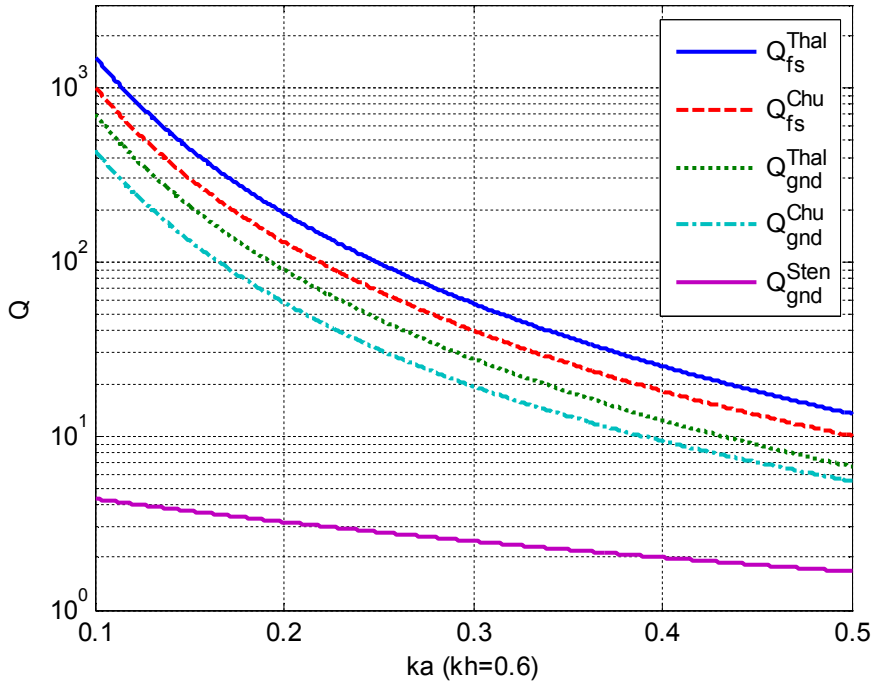

(a)

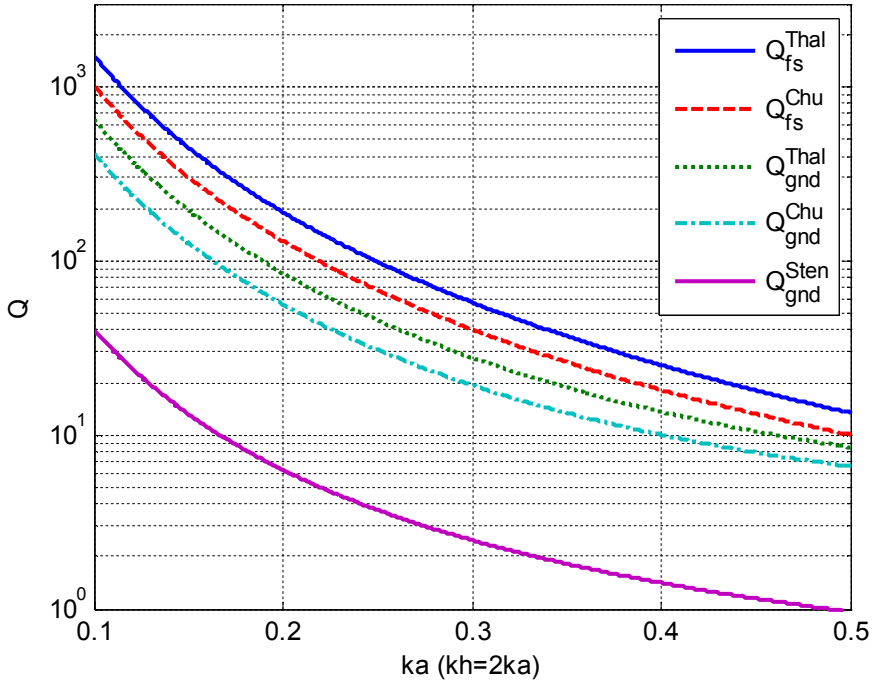

(b)

Figure 12: Comparison of quality factors of antennas. (a) Quality factors of antennas in free space and those above a ground with a separation kh=0.6. (b) The comparison of quality factors of free-space antennas and grounded antennas with a fixed ratio kh=2ka. In both cases, the quality factor from [10] is also shown for comparison.

Figures 12(a) and 12(b) show the results of those four quality factors and compare them in the range of *ka* from 0.1 to 0.5. Figure 12(a) is the comparison between the quality factors of free-space antennas and the quality factors of grounded antennas with a fixed ground separation (kh=0.6). Figure 12(b) compares the quality factors for free-space antennas and the quality factors of antennas above a PEC ground plane with a fixed ratio (kh=2ka) between the ground separation (kh) and the antenna size (ka). Due to the exclusion of the energy inside the sphere, Q_{fs}^{Chu} is smaller than Q_{fs}^{Thal}. In free space, Chu's quality factor is the lower bound for the antenna. However, according to Figures 12(a) and 12(b), it is observed that Q_{gnd}^{Chu} and Q_{gnd}^{Thal} are both lower than Q_{fs}^{Chu}. In other words, placing a spherical antenna above a PEC ground plane can reduce the quality factor. This means the bandwidth of a spherical antenna can be wider than that of a same-sized electrically small antenna in free space. In either configuration, Chu's quality factor represents a fundamental lower bound that no quality factors of physical antennas can go below. However, electrically small antenna designs have been reported that have the radiation Q closely approaching Q_{fs}^{Thal} [7]. Therefore, it is interesting to note that Q_{gnd}^{Thal} is expected to be smaller than Q_{fs}^{Chu}. In both Figures 12(a) and 12(b), the purple curves are from [10]. They are significantly low and cannot be reached in practice.

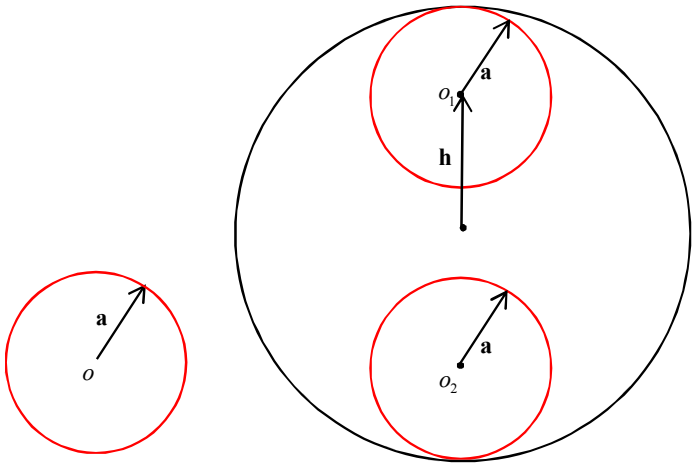

(a) (b)

Figure 13: Comparison of effective volumes. (a) A spherical antenna is placed in free space. (b) Two spherical antennas are placed in free space.

The quality factor for the TM_{01} mode is well-known. When the radius of enclosed surface increases, the minimum quality factor decreases. Figure 13(a) is a spherical antenna placed in free space. Figure 13(b) is the system after the image theory is applied. Those three antennas are identical. It is easy to see the radius a of the spherical antenna in Figure 13(a),is smaller than the radius $h+a$ of the sphere enclosing both the original and image antennas in Figure 13(b). Hence, the fundamental lower bound of Q for the two-antenna system in Figure 13(b) is lower than that for the single antenna in Figure 13(a). As reported in [10], such a bound is too conservative and it cannot be closely approached using physical antennas. In contrast, the results in Figure 12 show Q values that may be realized using physical antenna designs.

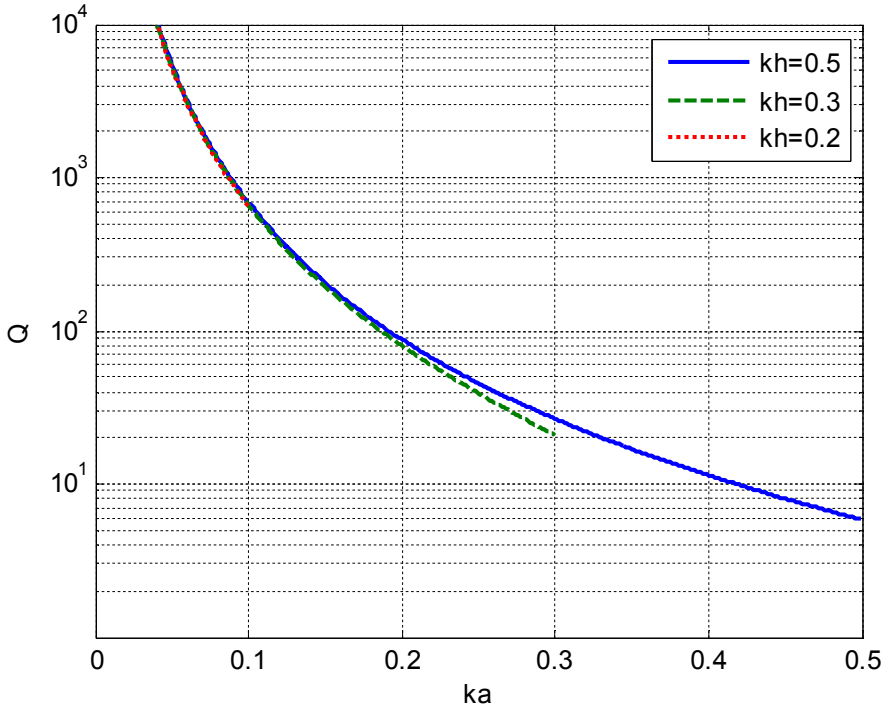

(a)

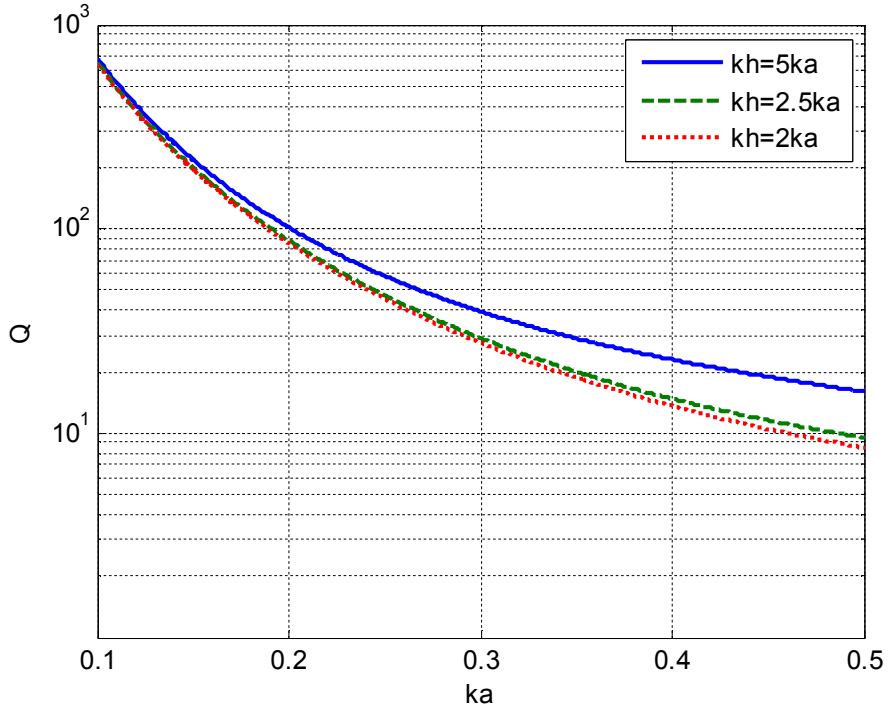

(b)

Figure 14: Quality factors for grounded antennas. (a) Quality factor Q_{gnd}^{Chu} with respect to *ka* with fixed *kh*. (b) Quality factor Q_{gnd}^{Chu} with respect to *ka* with fixed ratios between *ka* and *kh*.

Figure 14(a) shows Q_{gnd}^{Chu} as a function of *ka* for fixed values of *kh*. Figure 14(b) plots Q_{gnd}^{Chu} with respect to *ka* for fixed values of the ratio *kh*/*ka*. From Figures 14(a) and 14(b), the quality factor with a fixed separation (*kh*) decreases when the antenna size (*ka*) increases, as expected; a larger antenna has a smaller quality factor. Moreover, when the separation increases for a fixed antenna size (*ka*) the quality factor increases.

The quality factor can be lower than Chu's limit if a PEC ground plane is present. The ground plane can influence the quality factor significantly. The impact decreases when the separation increases. When the antenna is far away from the PEC ground plane, the quality factor is expected to be close to the quality factor in free space.

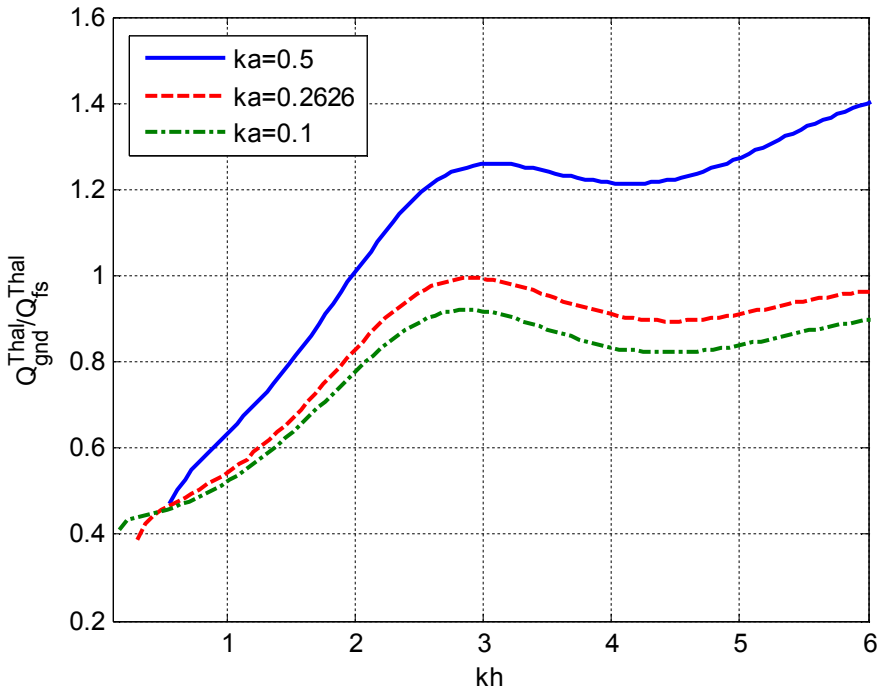

Figure 15: The ratios of quality factors for grounded antennas to those of free-space antennas with respect to the separation (*kh*) for different antenna sizes (*ka*).

The ratio of quality factors $Q_{gnd}^{Thal} / Q_{fs}^{Thal}$ serves as a useful figure of merit. This quantity will be very close to unity if the separation is large. According to Figure 15, the values of green (ka=0.1) and red (ka=0.2626) curves are close to unity when kh is larger than three. Beyond three, the ratios stay around unity. At lower values of kh, it is observed that Q_{gnd}^{Thal} approaches Q_{fs}^{Thal} when the separation increases. It is another indicator that the influence of the PEC ground plane on antenna bandwidth decreases when the ground separation increases.

To understand more about the stored energy and radiated power behavior when the separation changes, we define the ratio of stored energy, $W_{gnd}^{Thal} / W_{fs}^{Thal}$, and ratio of radiated power, $P_{gnd}^{Thal} / P_{fs}^{Thal}$. Here, W_{gnd}^{Thal} is the stored energy including the energy inside the spherical antenna with a PEC ground plane; W_{fs}^{Thal} is the stored energy including the energy inside the spherical antenna in free space; P_{gnd}^{Thal} is the radiated power with a PEC ground; and P_{fs}^{Thal} is the radiated power in free space.

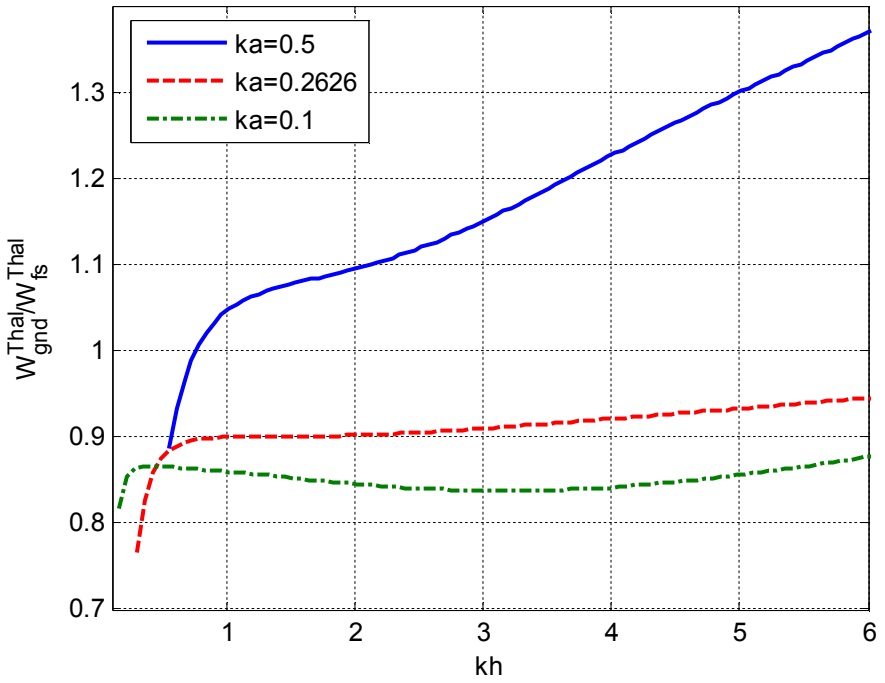

(a)

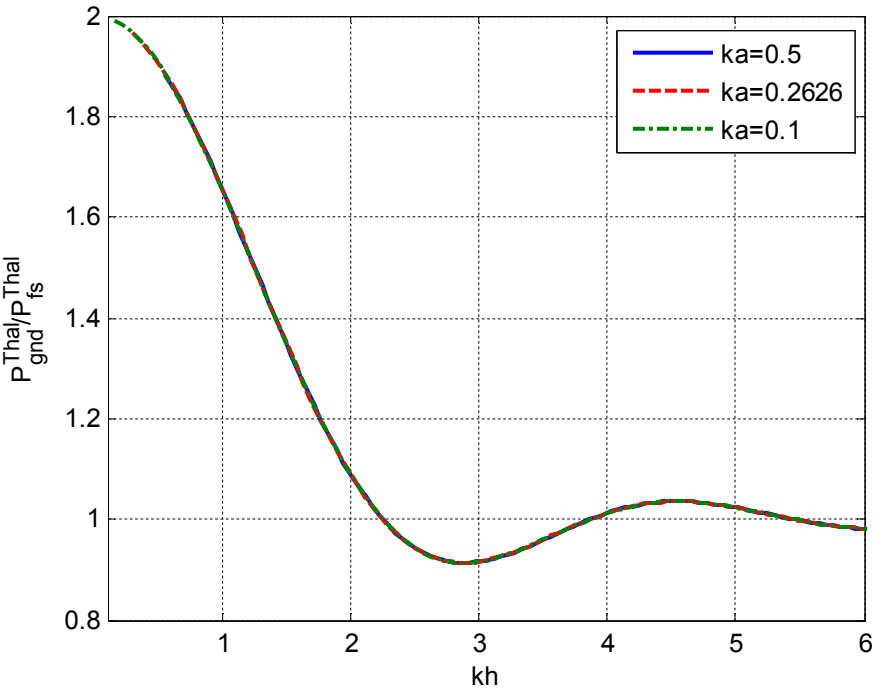

(b)

Figure 16: Comparison of stored energy and radiated power. (a) The ratios of stored energy with respect to the separation (*kh*). (b) The ratios of the radiated power with respect to the separation (*kh*).

Figures 16(a) and (b) compare the powers and stored energies between the free-space and grounded antenna cases. From Figure 16(a), when the separation is small, the stored energy with a PEC ground plane, W_{gnd}^{Thal}, is smaller than the stored energy in free space, W_{fs}^{Thal}. In this case, a PEC ground plane reduces the stored energy. The influence decreases, *i.e.* W_{gnd}^{Thal} approaches W_{fs}^{Thal}, by increasing the separation. However, a different trend is observed for the radiated power. Since the image theory is used, there are two spherical antennas in free space with a separation, $2h$. When kh is small, the two antennas appear to be at the same location viewed from far field region. The vector fields from the two antennas coherently add in every direction, when observed in the far zone. Hence, the radiated power with a PEC ground plane should be four times larger than the radiated power in free space. However, since the image theory is only valid in the upper hemisphere, the total radiated power should be divided by two. Figure 16(b) shows that when kh is small, $P_{gnd}^{Thal} / P_{fs}^{Thal}$ is around two. Again, the influence of the PEC ground plane on the radiated power decreases when the separation increases. The ratio is close to unity when kh is large in Figure 16(b).

For small ground separations, the stored energy for a grounded antenna is smaller than that of a free-space antenna ($W_{gnd}^{Thal} < W_{fs}^{Thal}$), and the radiated power is two times larger than

the radiated power in free space ($P_{gnd}^{Thal} \Big/ P_{fs}^{Thal} \approx 2$). Hence, the quality factor decreases when a PEC ground plane is placed for small ground separations.

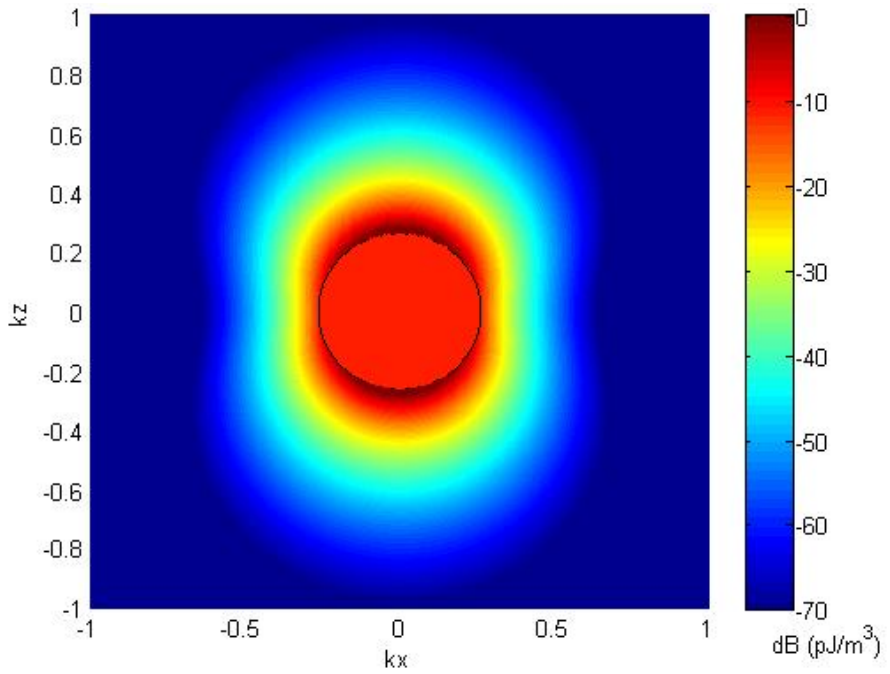

(a)

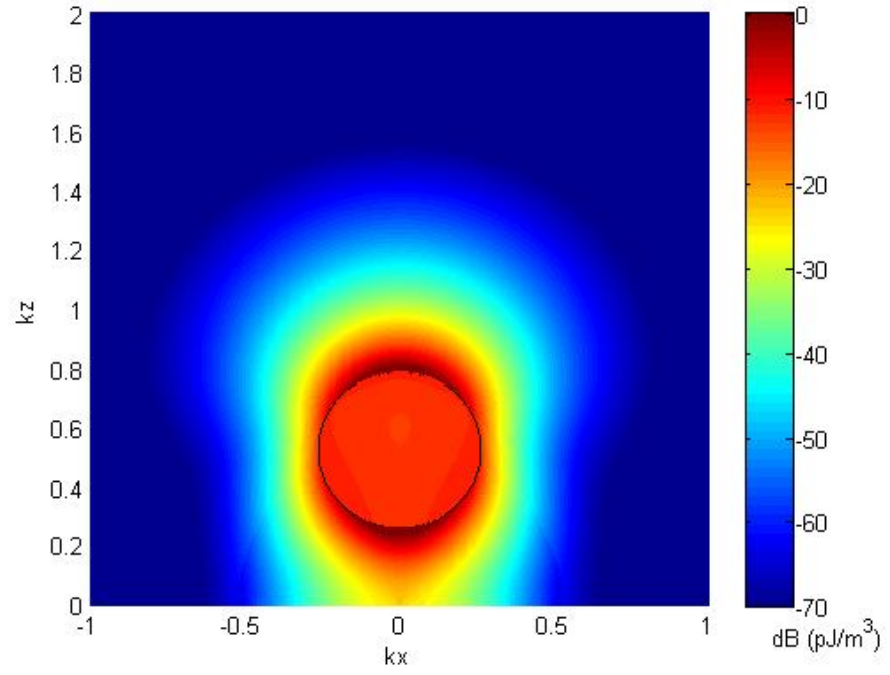

(b)

Figure 17: Non-propagating energy densities. (a) Energy density of the antenna in free space. (b) Energy density of the antenna above a PEC ground plane. The distributions are rotationally symmetric around the *z*-axis.

To understand more about the PEC ground plane influence of stored energy, we take a close look at the energy density distribution. Figure 17(a) shows the non-propagating energy density distribution of the antenna in free space. The maximum of the energy density is at kx=0. The energy density distribution is symmetric to kx=0. From Figure 17(a), it is observed that the energy concentrates inside the antenna and in the region close to the antenna. The energy density decays very fast in outside region. In Figure 17(b), the PEC ground plane is placed at the kz=0 plane. The separation between the PEC ground plane and the antenna is 0.5252. The center of the antenna is at (kx,kz)=(0,0.5252).

According to Figure 8, there is a boundary between region II and region III. In regions I and II, the fields are written in standing waves, where there is no energy associated with radiation. In regions III and IV, the fields are written in propagating waves. The electric stored energy is equal to the total electric energy less the electric energy associated with radiation. In addition, the energy density is discontinuous across this boundary between regions II and III. As Figure 8 shows, the radius of this boundary is equal to the separation between the antenna and the PEC ground plane. The discontinuity in energy density is visible in Figure 17(b) across this boundary at radius 0.5252 measured from the coordinate origin.

Comparing Figure 17(a) and Figure 17(b), it can be observed that the energy density is not changed significantly by the PEC ground plane. Resultantly, the total electric stored energy is not changed significantly by PEC ground plane. However, the radiated power changes significantly, as shown in Figure 16(a). The ratio $P_{gnd}^{Thal} \big/ P_{fs}^{Thal}$ approaches 0.9 when *kh* is equal to 0.5252.

CHAPTER 5

VALIDATION WITH ANTENNA SIMULATION

Several antennas that closely approach Q_{fs}^{Thal} have been reported in the literature. Best [7], [8] designed a 4-arm folded spherical helix antenna with an air core inside. Both simulation and measurement results have been presented. The tuned antenna's quality factor can also be determined directly from the antenna's untuned feed point impedance, (3).

Table 1: The resonant antenna's properties in free space.

Number of Arms	Resonant Frequency (MHz)	Resonant Resistance (Ohms)	Q_{fs}^{imp}	Q_{fs}^{Thal}
4	300.07	46.38	90.17	85.32

Table 1 shows the properties of the helix spherical antenna with the resonant frequency at 300 MHz [7]. At the design frequency, the antenna has an electrical size of ka=0.2626. From the frequency-dependent input impedance (3), the quality factor is 90.17. According to [6], the theoretical quality factor is 85.32.

To confirm the theoretical result from Chapter 3, several folded spherical helix antennas based on [7] were simulated. Their quality factors were obtained from the input

impedance and then compared with the theoretical results in Chapter 4. The spherical helix antenna is placed above a PEC ground plane in the *x*-*y* plane with a separation, *kh*, *i.e.* the center of the antenna was placed at (*x*,*y*,*z*)=(0,0,*h*). The radius of the spherical antenna is 4.18 cm and the antenna resonates at 300 MHz. The number of turns of the spherical helix antenna was tuned to make it resonate at 300 MHz. The 4-arm spherical helix antenna operates as a folded dipole antenna with a predominantly vertically-polarized radiation pattern [7]. Since the antenna characteristics change when it is placed above a ground plane, a different number of arms from four and a continuously variable number of turns were used to obtain a good impedance match to 50Ω at resonance. The input port was placed at the center of one arm to excite the antenna.

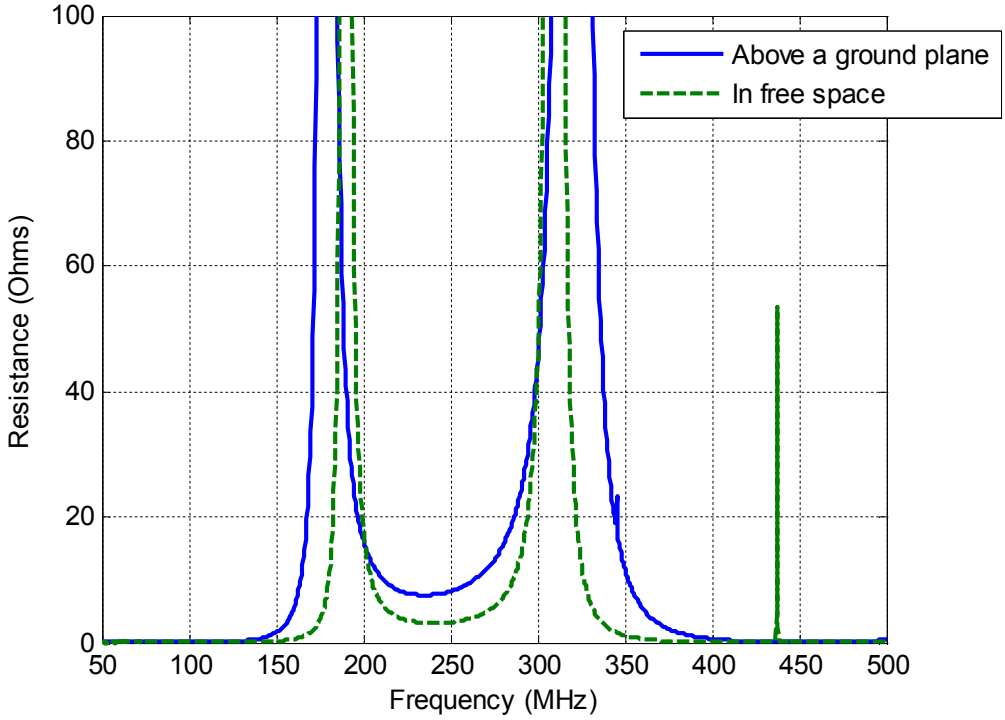
Above a ground plane
In free space
Resistance (Ohms)
Frequency (MHz)
0
20
40
60
80
100
50
100
150
200
250
300
350
400
450
500

(a)

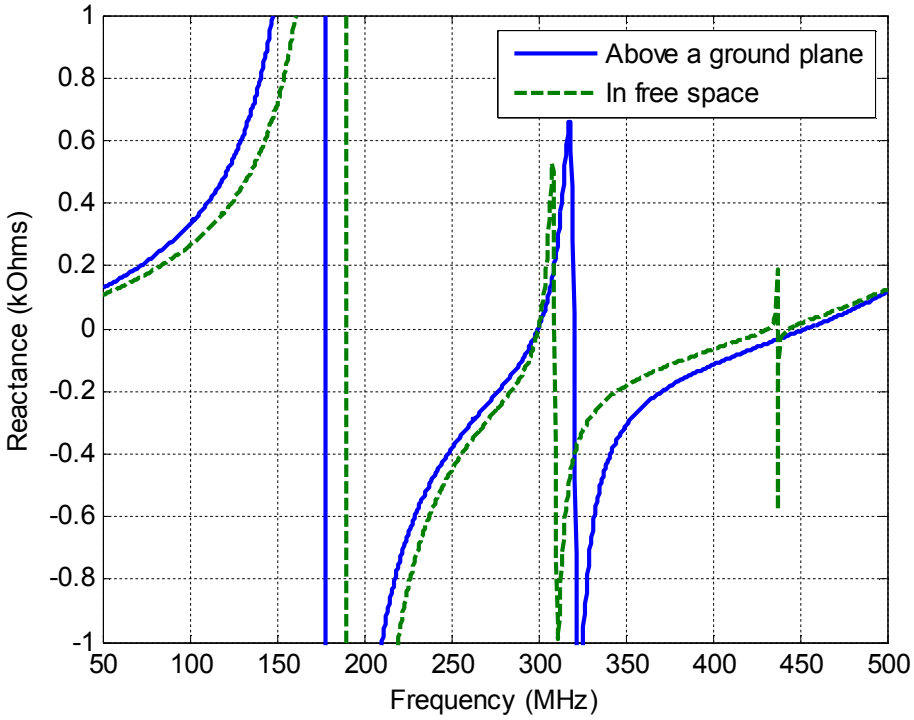
Above a ground plane
In free space
Reactance (kOhms)
Frequency (MHz)
1
0.8
0.6
0.4
0.2
0
-0.2
-0.4
-0.6
-0.8
-1
50
100
150
200
250
300
350
400
450
500

(b)

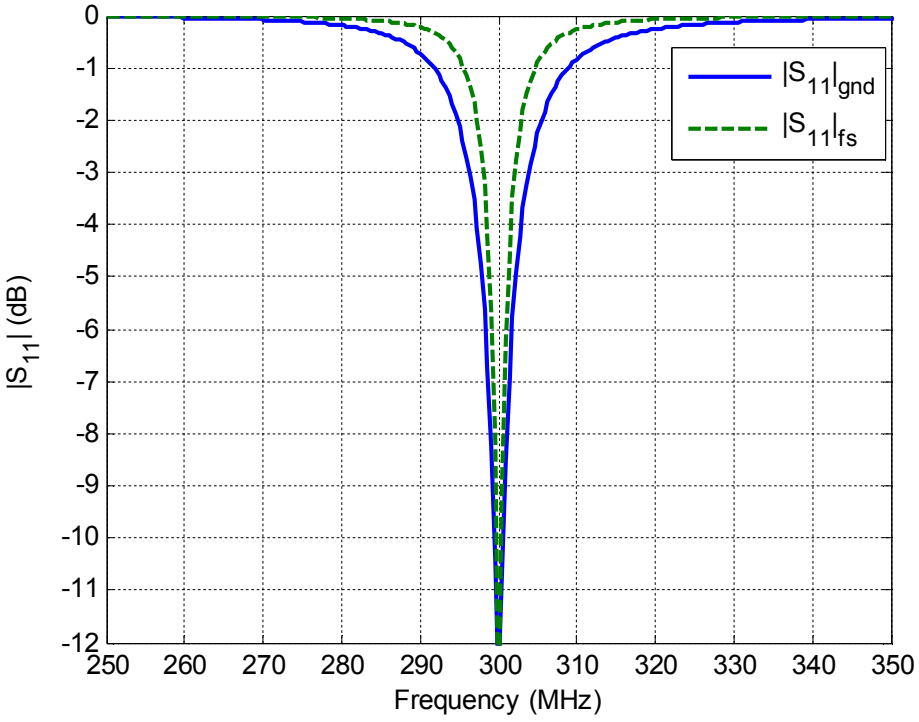

(c)

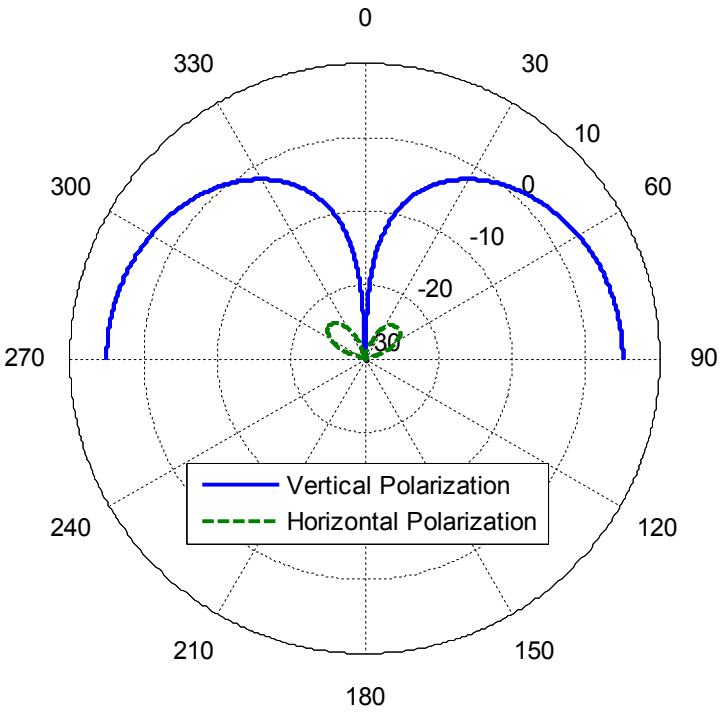

(d)

Figure 18: Impedance and radiation characteristics of spherical helix antennas in free space and above a ground plane. (a) The input resistance. (b) The input reactance. (c) The

input reflection coefficient. (d) Radiation pattern of the antenna above a ground plane. The electrical size of both antennas and the ground separation for the grounded antennas are given by ka=0.2626 and kh=0.5252.

Figures 18(a) and 18(b) compare the input impedance of the free-space antenna and the grounded antenna with respect to frequency for the same electrical antenna size ka=0.2626. For the grounded antenna, the ground separation is given by kh=0.5252. The trend and characteristic of the impedance curves are similar to those of the helix spherical antenna in free space [8]. Figure 18(c) shows a comparison of the input reflection coefficient $|S_{11}|$ for the two antennas. The 3-dB bandwidth of the spherical antenna in free space is 4.1 MHz (298.2–302.3 MHz) or 1.37%. The bandwidth of the spherical antenna above a PEC ground plane is 7.7 MHz (296.4–304.1MHz) or 2.57%. The impedance bandwidth almost doubled with the PEC ground plane. Figure 18(d) shows the E-plane directivity patterns of the grounded spherical antenna. It is observed that the horizontal polarization is about 25 dB below the vertical polarization, confirming that the spherical helix antenna above the ground plane is predominantly vertically polarized, consistent with the folded dipole model. Design specifications and the associated impedance and radiation characteristics of all spherical helix antennas above the ground plane presented in this study are listed in Appendix.

Table 2: The resonant antenna's properties above a PEC ground plane with different separation.

Number of Arms	Separation (*kh*)	Resonant Resistance (Ohms)	Q_{gnd}^{imp}	Q_{gnd}^{Thal}
3	0.5252	45.25	47.76	39.45
4	$\pi/2$	59.44	68.07	58.93
4	π	43.07	95.99	84.26
4	4.5	47.5	86.66	76.30
4	2π	45.48	88.77	82.54

Table 2 lists quality factors for different separations for the same antenna size *ka*=0.2626. The quality factor increases when the separation increases. The quality factor from simulation agrees with the theoretical result with small errors with the same trend — a PEC ground plane impacts the quality factor significantly and the influence decreases with increasing separation.

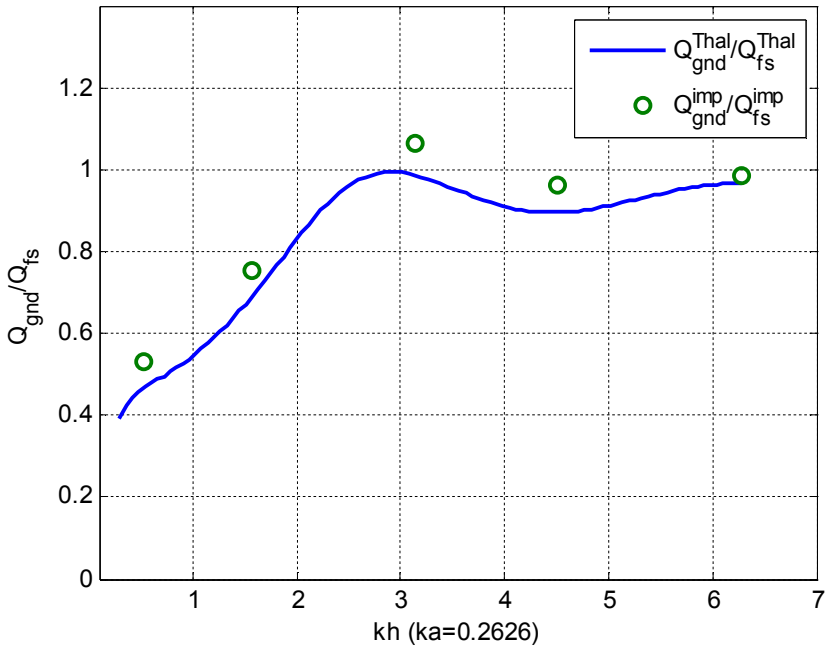

Figure 19: The comparison of simulation and theoretical results of the quality factor for the antenna size *ka*=0.2626 for different ground separations.

In Figure 19, the ratios $Q_{gnd}^{Thal}/Q_{fs}^{Thal}$ and $Q_{gnd}^{imp}/Q_{fs}^{imp}$ from the theory (blue line) and simulations (green dots) are compared. Overall, the simulated results follow the trend of the theoretical results. In the mathematical model, an impressed current was placed over the spherical surface. Here, no mutual coupling between the currents over the original antenna and image antenna surfaces is taken into account. However, the mutual coupling effect is taken into account in antenna simulations. The difference between the Q values is attributed in part to this mutual coupling effect between the original and image antennas. Note that the two Q values are close to each other for the largest separation $kh=2\pi$.

CHAPTER 6

CONCLUSION

In qualitative terms, it is well-known that in the presence of a PEC ground plane the quality factor, or the impedance bandwidth, of an antenna is affected, and especially so when the ground separation is small. Using image theory, the radiation quality factors of small vertically polarized antennas above a PEC ground plane were investigated using a two-antenna configuration in free space. For small ground separations, it was found that the presence of a ground plane not only reduces the energy stored in the antenna, but also doubles radiated power, compared with a single antenna of the same size in free space. This reduces the quality factor of a small antenna above a PEC ground plane to a value lower than that of the same antenna in free space.

A larger effective volume of an antenna results in a lower quality factor or a broader impedance bandwidth. The effective volume of a antenna in free space is the volume of the antenna itself. Placing an antenna above a PEC ground plane makes the effective volume larger due to the image antenna below the ground plane. Therefore, an electrically small antenna above a ground plane has the potential of having a broader bandwidth compared with the antenna of the same size in free space. This study provides

a theoretical basis that this bandwidth increase is indeed possible with a ground plane for vertically polarized antennas. Furthermore, the amount of decrease in Q has been quantified as a function of antenna size and ground separation.

Using full-wave simulations of folded spherical helix antennas above a ground plane, it has been shown that the antenna's quality factor can be lower than the Chu lower bound on Q in free space when placed above a PEC ground plane for electrically small antenna sizes (ka<0.5) and ground separations (kh<0.5). The impact of the PEC ground plane on the antenna Q decreases with increasing ground separation. At large ground separations, the impedance bandwidth will approach that of the antenna in free space as expected.

APPENDIX

ANTENNA SIMULATIONS

1. Antenna size *ka*=0.1166 and resonant frequency *f*=133 MHz

1.1 *kh*=0.2332

Table 3: The resonant 5-arm helix antenna's properties above a PEC ground plane.

Number of Arms	Number of Turns	Total Wire Length (cm)	Number of Sections of a Arm	Q_{gnd}^{imp}
5	3.8	147.803	48	424.5

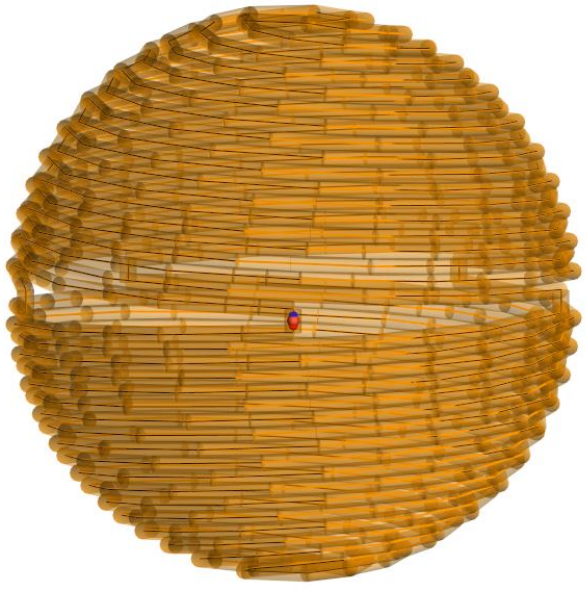

(a)

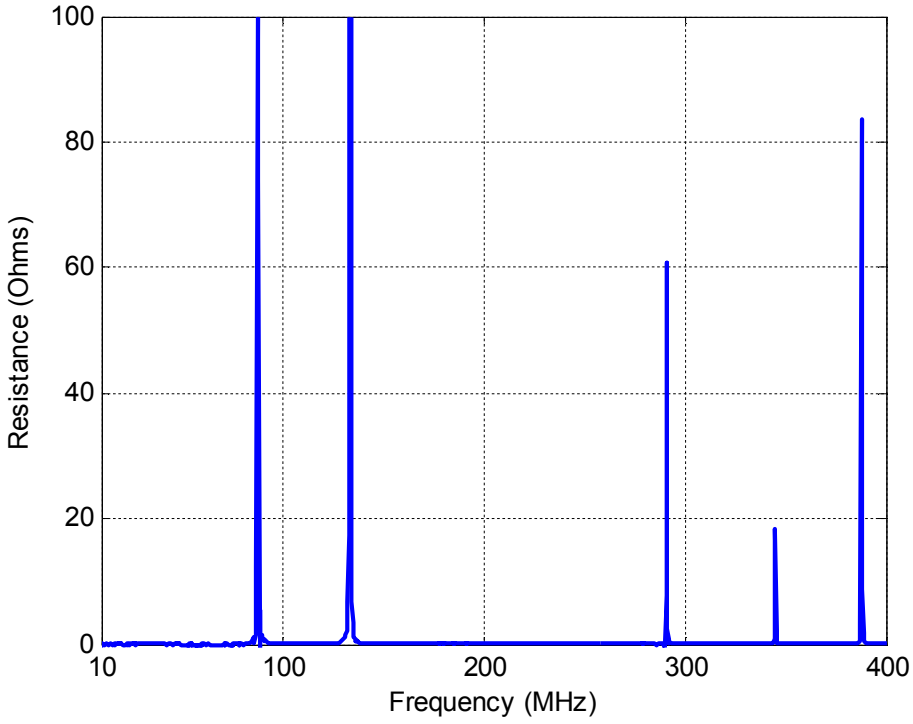
Resistance (Ohms)
Frequency (MHz)
100
80
60
40
20
0
10
100
200
300
400

(b)

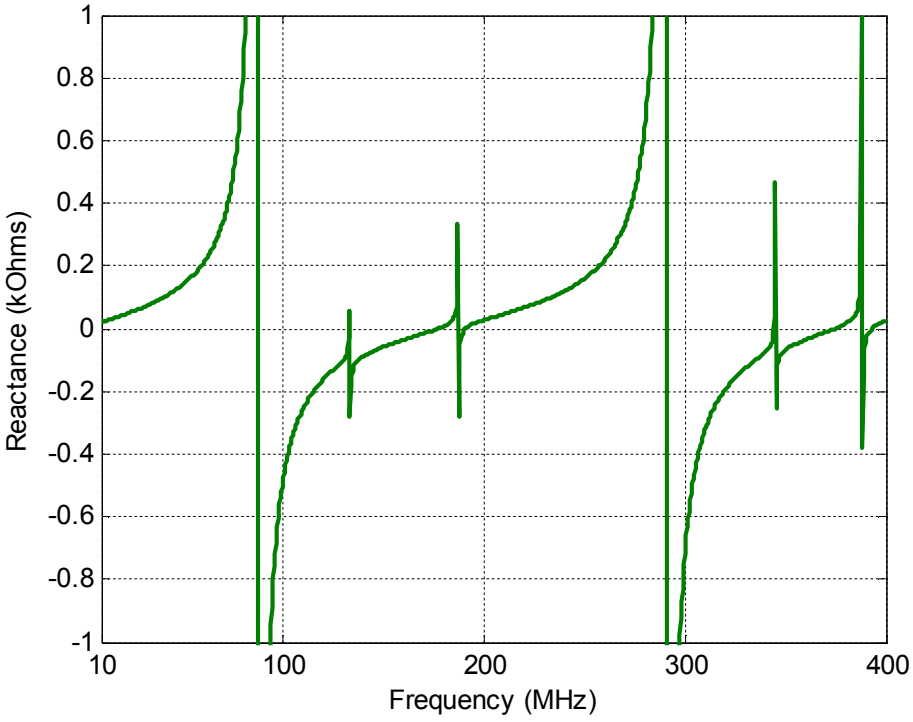
Reactance (kOhms)
Frequency (MHz)
1
0.8
0.6
0.4
0.2
0
-0.2
-0.4
-0.6
-0.8
-1
10
100
200
300
400

(c)

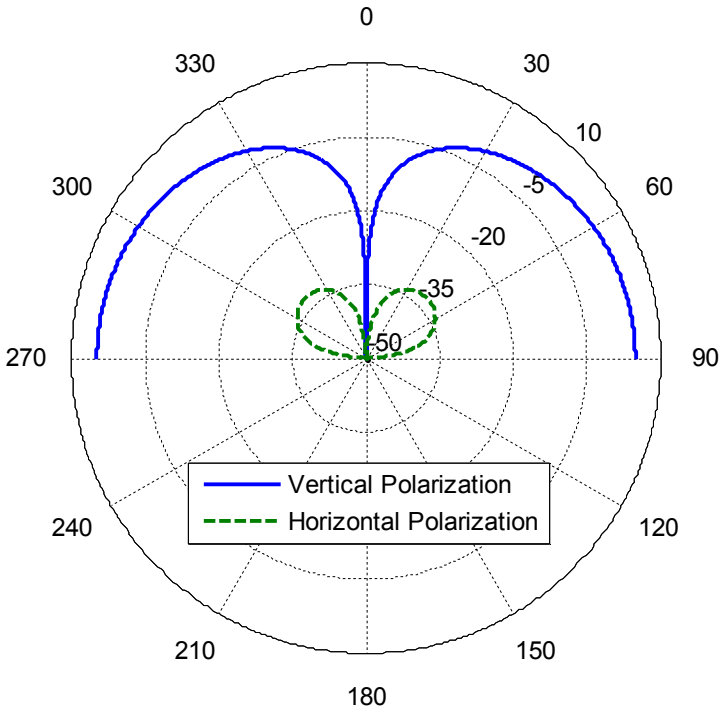

(d)

Figure 20: Geometry and electrical characteristics of an antenna with *ka*=0.1166 for ground separation *kh*=0.2332. (a) The 5-arm spherical helix antenna geometry. (b) Input resistance with respect to frequency. (c) Input reactance with respect to frequency. (d) Radiation pattern at *f*=133 MHz.

2. Antenna size *ka*=0.2626 and resonant frequency *f*=300 MHz

2.1 *kh*=0.5252

Table 4: The resonant 3-arm helix antenna's properties above a PEC ground plane.

Number of Arms	Number of Turns	Total Wire Length (cm)	Number of Sections of a Arm	Q_{gnd}^{imp}
3	1.5883	64.0788	48	47.76

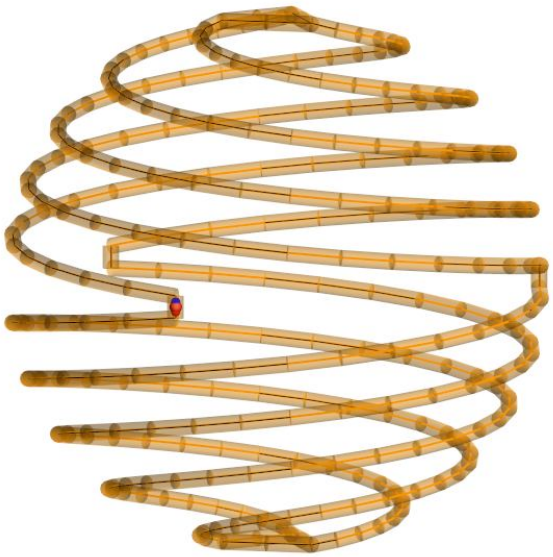

(a)

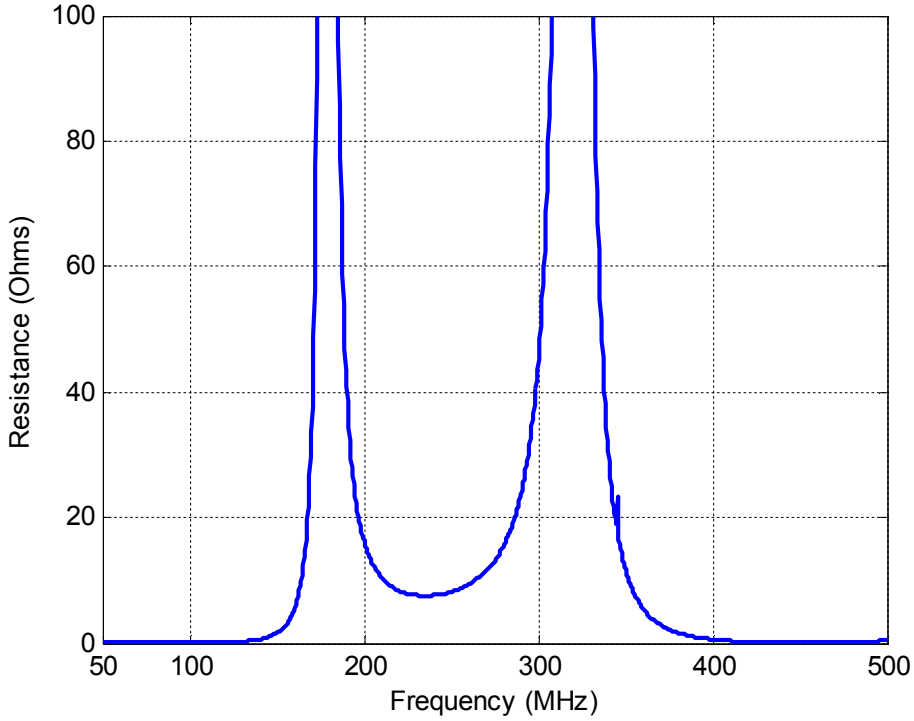
100
80
60
40
20
0
50
100
200
300
400
500
Resistance (Ohms)
Frequency (MHz)

(b)

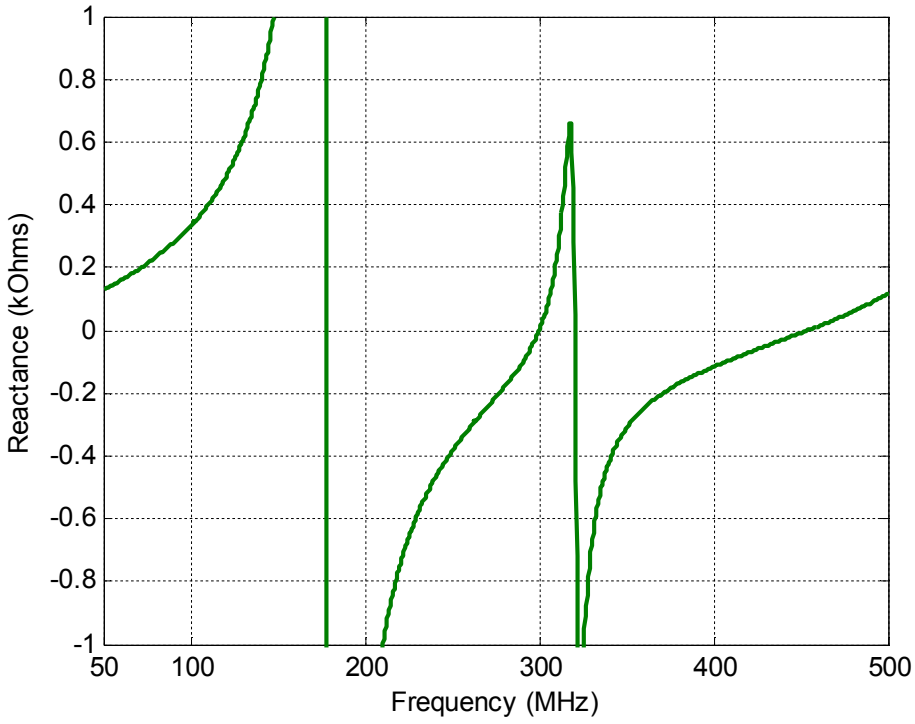

(c)

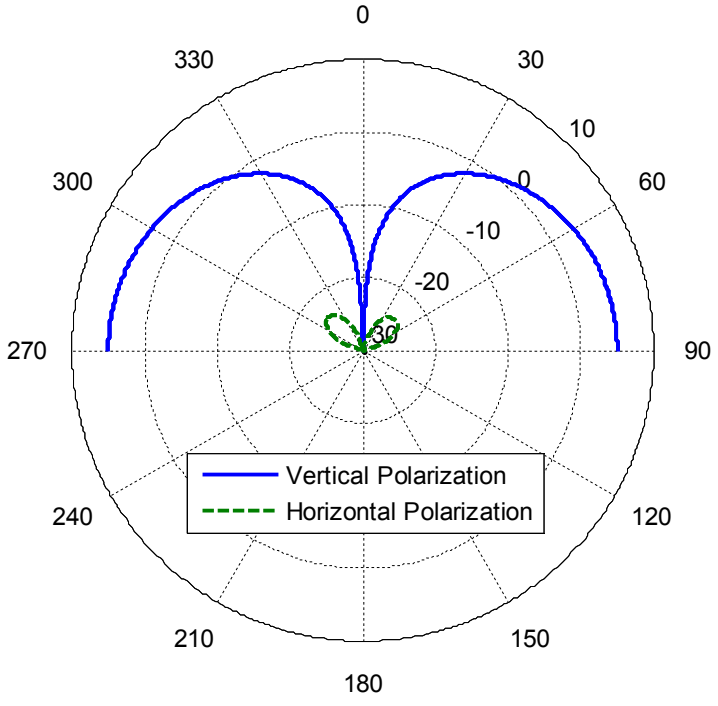

(d)

Figure 21: Geometry and electrical characteristics of an antenna with *ka*=0.2626 for ground separation *kh*=0.5252. (a) The 3-arm spherical helix antenna. (b) Resistance with

respect to frequency. (c) Reactance with respect to frequency. (d) Radiation pattern at f=300 MHz.

2.2 kh=0.5π

Table 5: The resonant 4-arm helix antenna's properties above a PEC ground plane.

Number of Arms	Number of Turns	Total Wire Length (cm)	Number of Sections of a Arm	Q_{gnd}^{imp}
4	1.635	65.8462	48	58.93

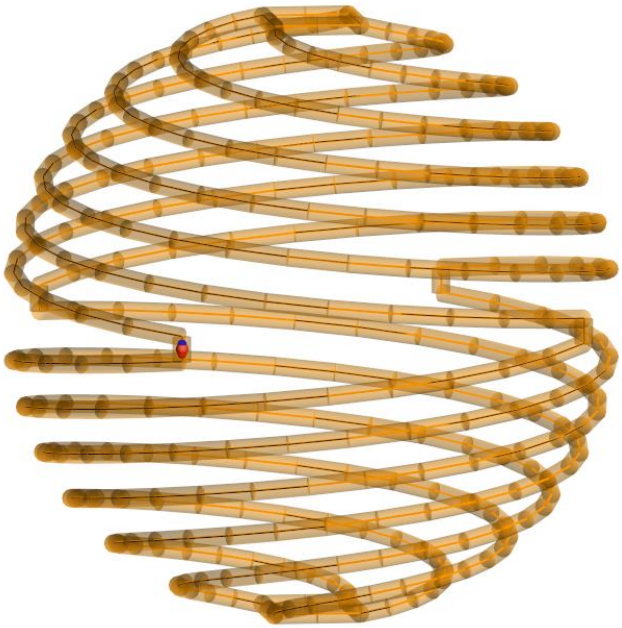

(a)

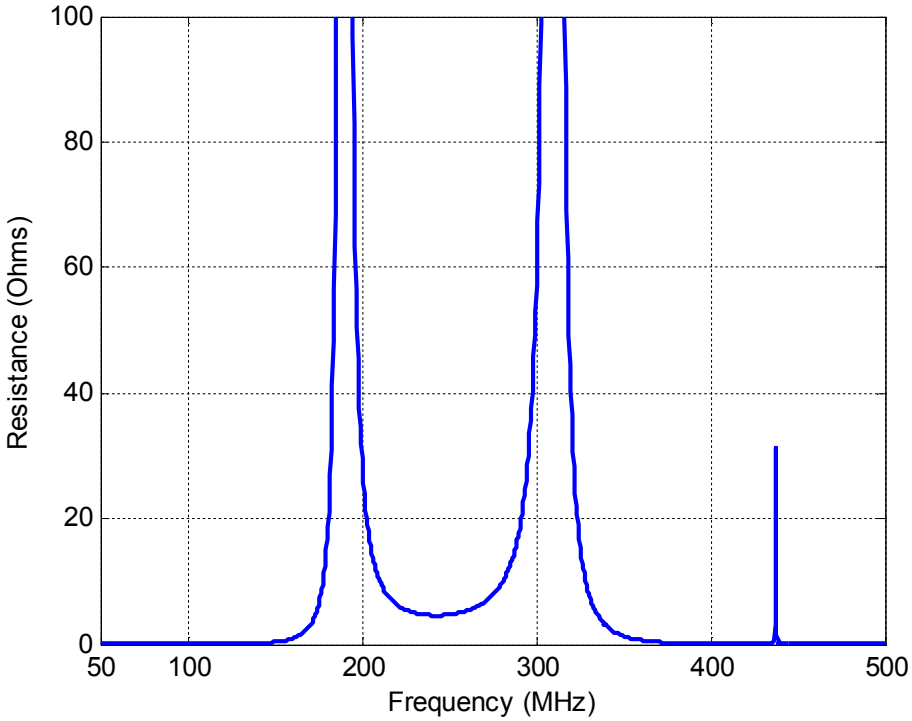
Resistance (Ohms)
Frequency (MHz)
100
80
60
40
20
0
50
100
200
300
400
500

(b)

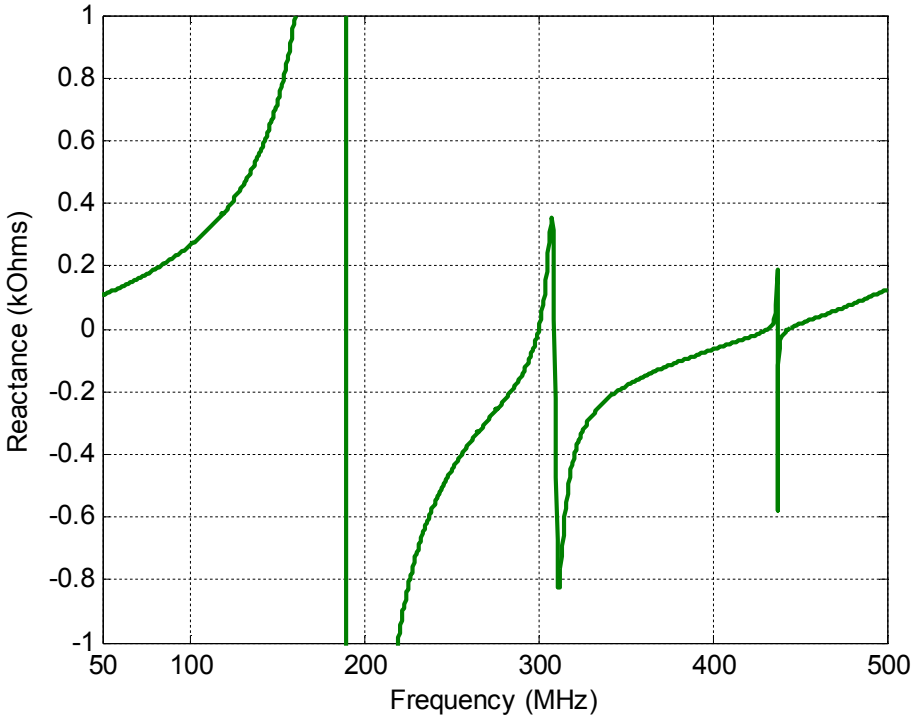
Reactance (kOhms)
Frequency (MHz)
1
0.8
0.6
0.4
0.2
0
-0.2
-0.4
-0.6
-0.8
-1
50
100
200
300
400
500

(c)

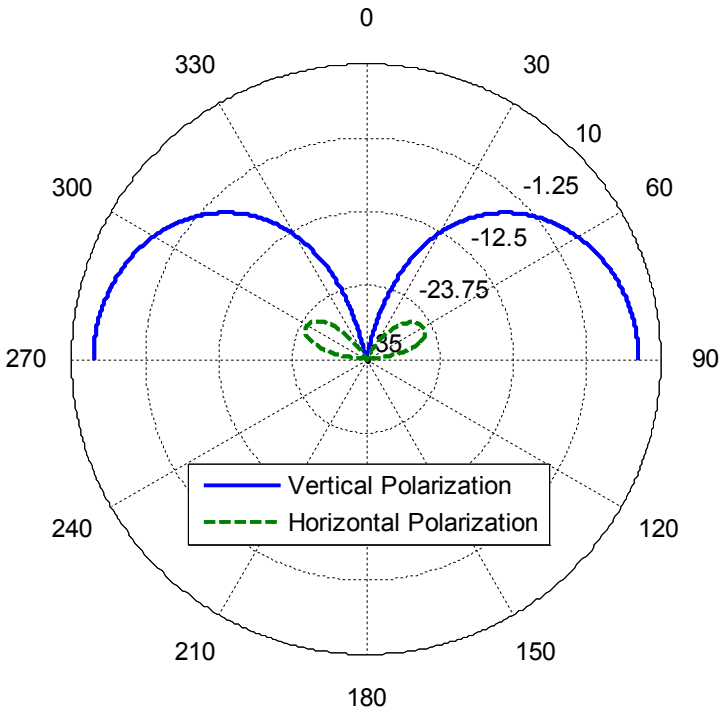

(d)

Figure 22: Geometry and electrical characteristics of an antenna with ka=0.2626 for ground separation kh=0.5π. (a) The 4-arm spherical helix antenna. (b) Resistance with respect to frequency. (c) Reactance with respect to frequency. (d) Radiation pattern at f=300 MHz.

2.3 $kh=\pi$

Table 6: The resonant 4-arm helix antenna's properties above a PEC ground plane.

Number of Arms	Number of Turns	Total Wire Length (cm)	Number of Sections of a Arm	Q_{gnd}^{imp}
4	1.635	65.8462	48	95.99

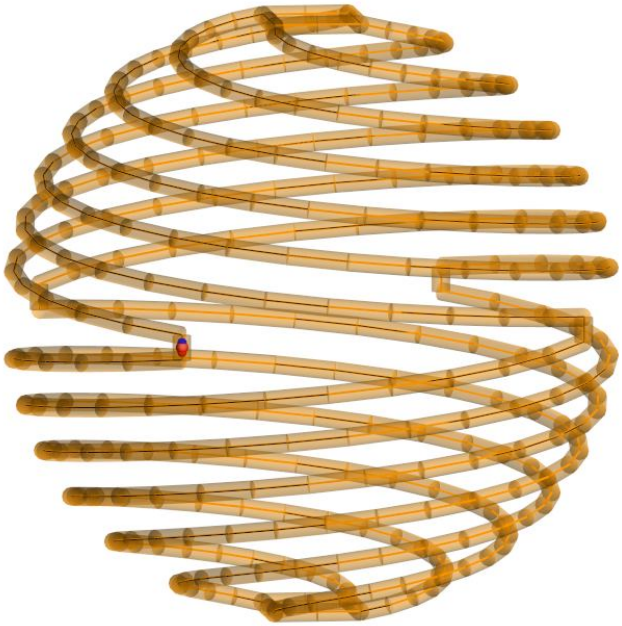

(a)

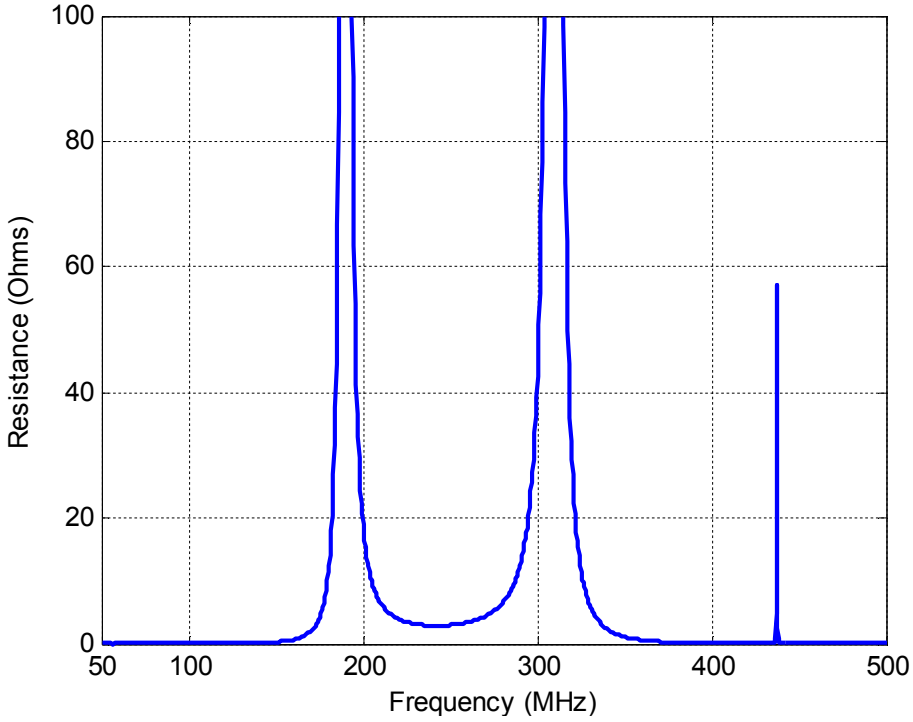
100
80
60
40
20
0
Resistance (Ohms)
50
100
200
300
400
500
Frequency (MHz)

(b)

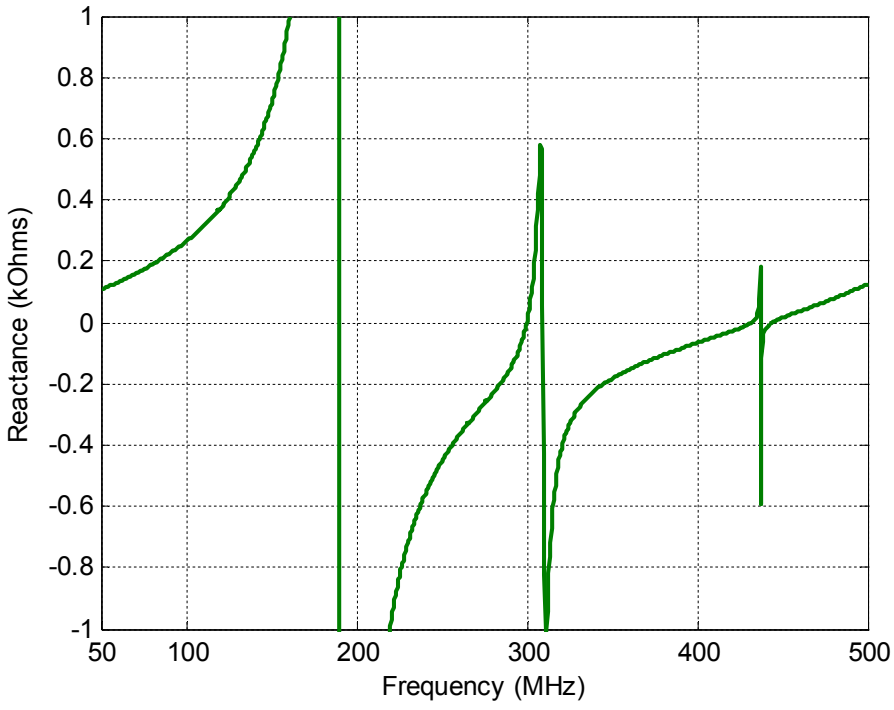

(c)

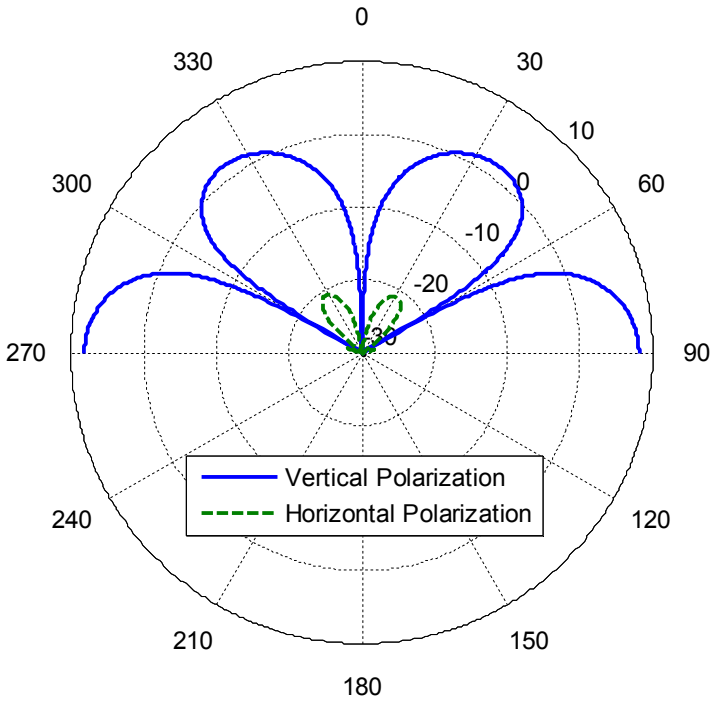

(d)

Figure 23: Geometry and electrical characteristics of an antenna with ka=0.2626 for ground separation kh=π. (a) The 4-arm spherical helix antenna. (b) Resistance with respect to frequency. (c) Reactance with respect to frequency. (d) Radiation pattern at f=300 MHz.

2.4 *kh*=4.5

Table 7: The resonant 4-arm helix antenna's properties above a PEC ground plane.

Number of Arms	Number of Turns	Total Wire Length (cm)	Number of Sections of a Arm	Q_{gnd}^{imp}
4	1.635	65.8462	48	86.66

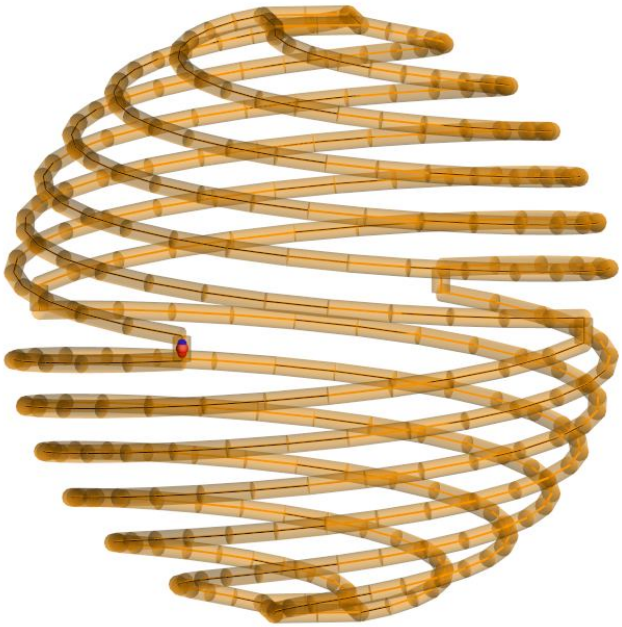

(a)

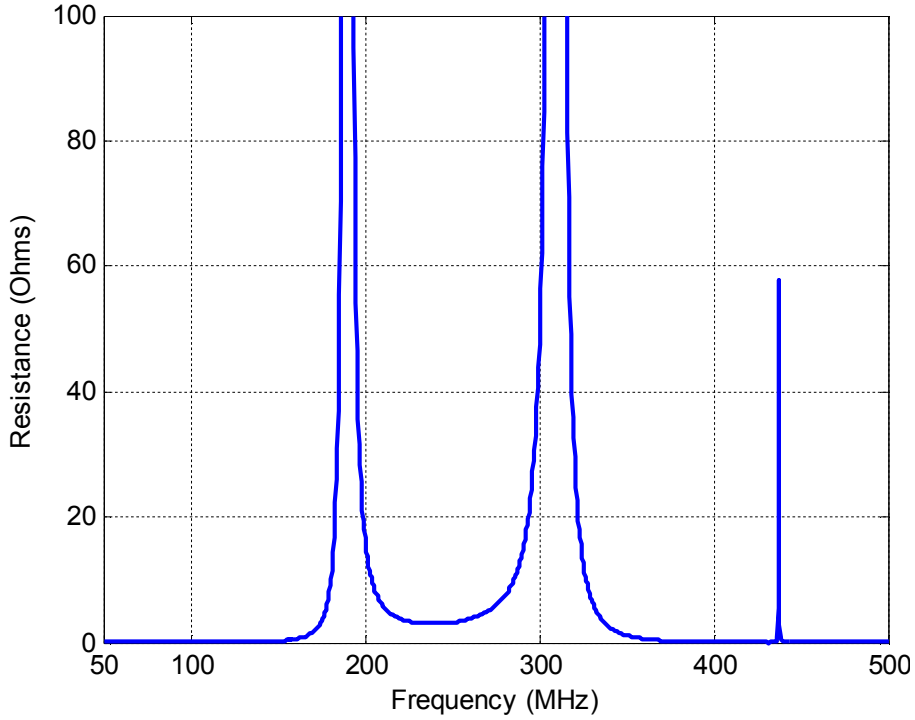
Resistance (Ohms)
Frequency (MHz)
100
80
60
40
20
0
50
100
200
300
400
500

(b)

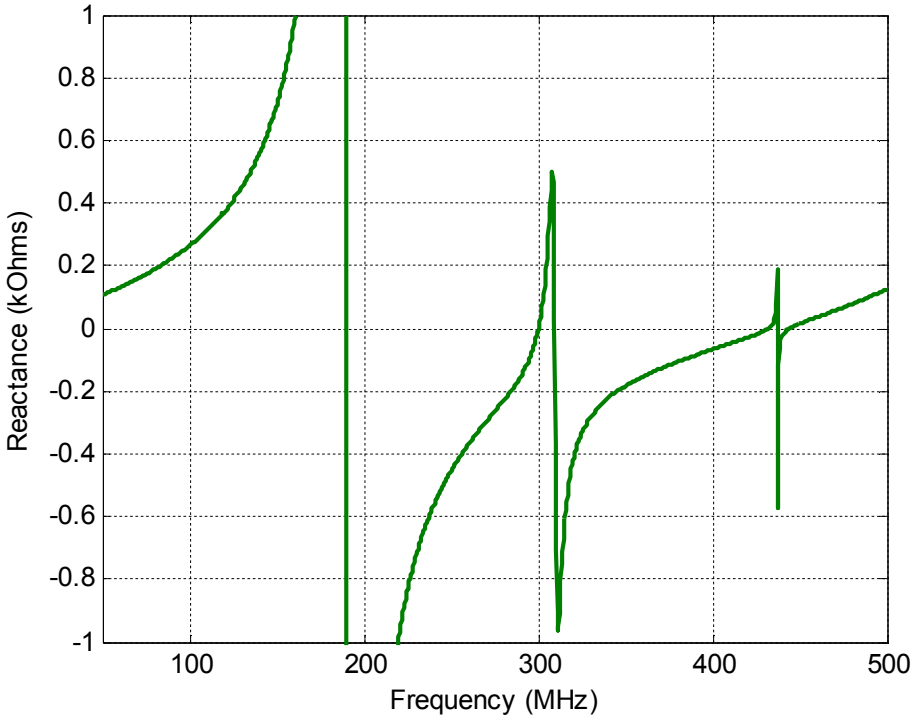
Reactance (kOhms)
Frequency (MHz)
1
0.8
0.6
0.4
0.2
0
-0.2
-0.4
-0.6
-0.8
-1
100
200
300
400
500

(c)

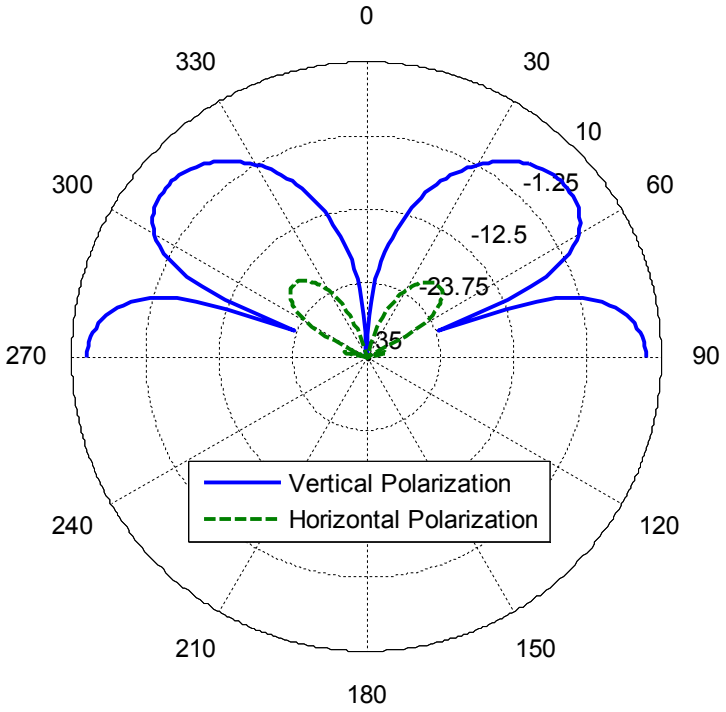

(d)

Figure 24: Geometry and electrical characteristics of an antenna with *ka*=0.2626 for ground separation *kh*=4.5. (a) The 4-arm spherical helix antenna. (b) Resistance with respect to frequency. (c) Reactance with respect to frequency. (d) Radiation pattern at *f*=300 MHz.

2.5 $kh=2\pi$

Table 8: The resonant 4-arm helix antenna's properties above a PEC ground plane.

Number of Arms	Number of Turns	Total Wire Length (cm)	Number of Sections of a Arm	Q_{gnd}^{imp}
4	1.635	65.8462	48	88.77

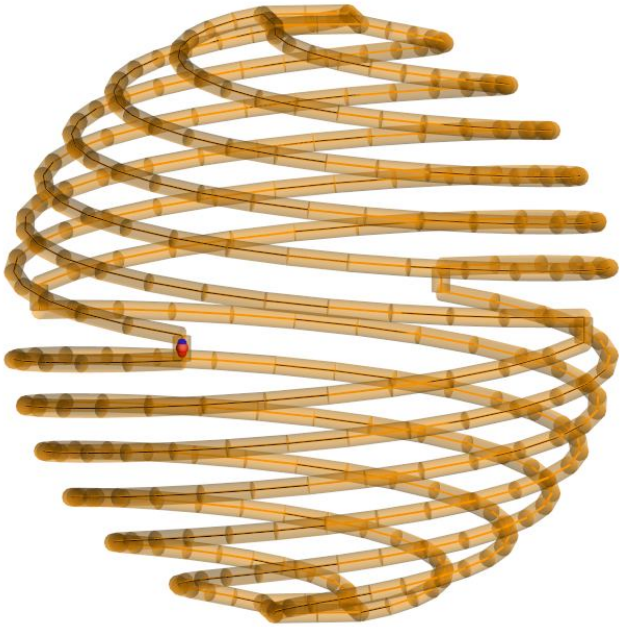

(a)

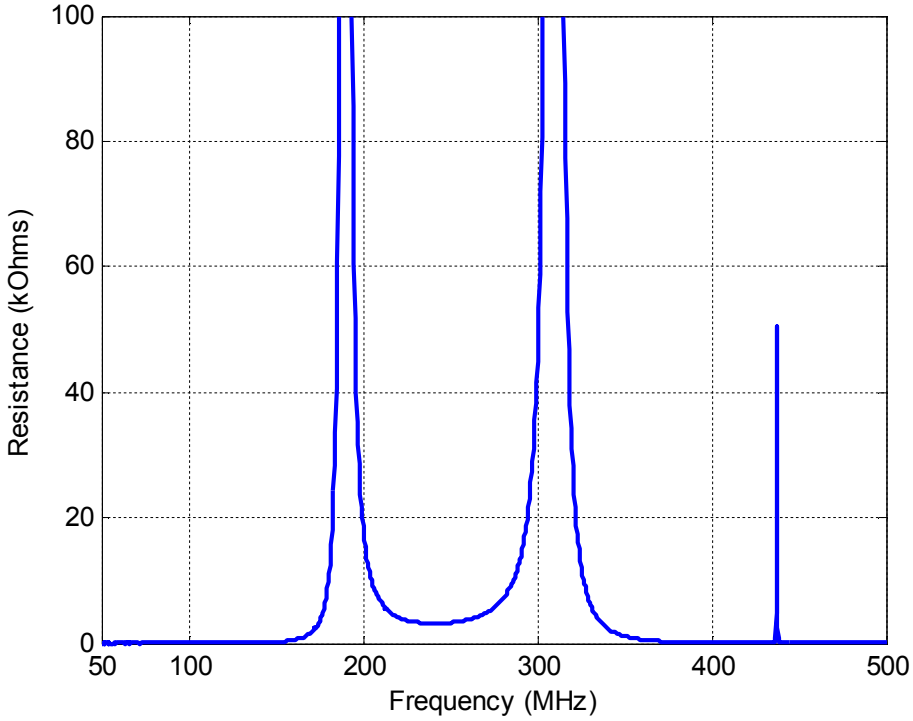
100
80
60
40
20
0
Resistance (kOhms)
50
100
200
300
400
500
Frequency (MHz)

(b)

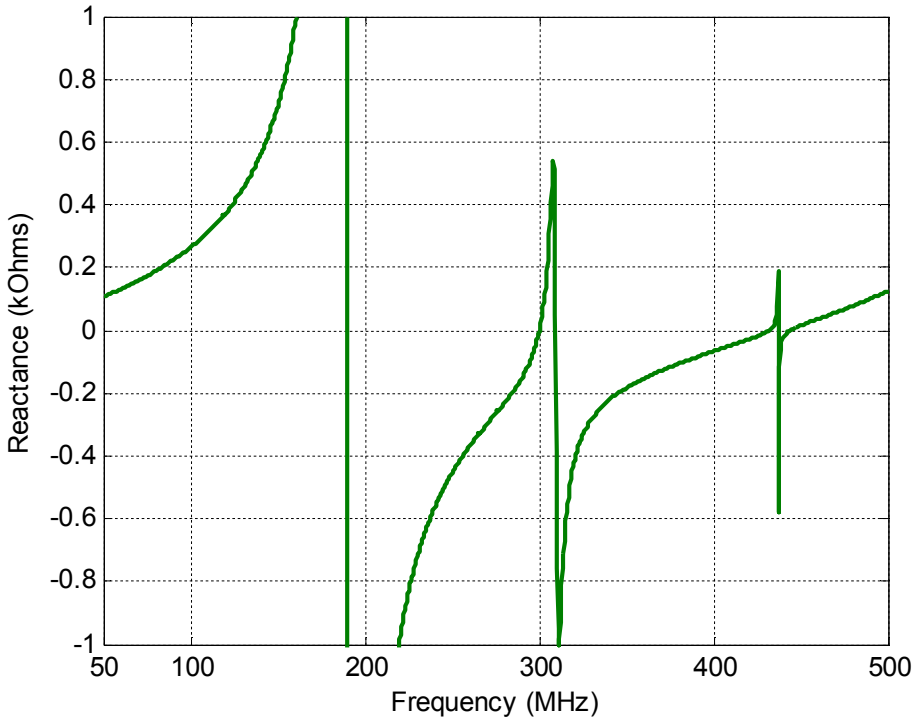

(c)

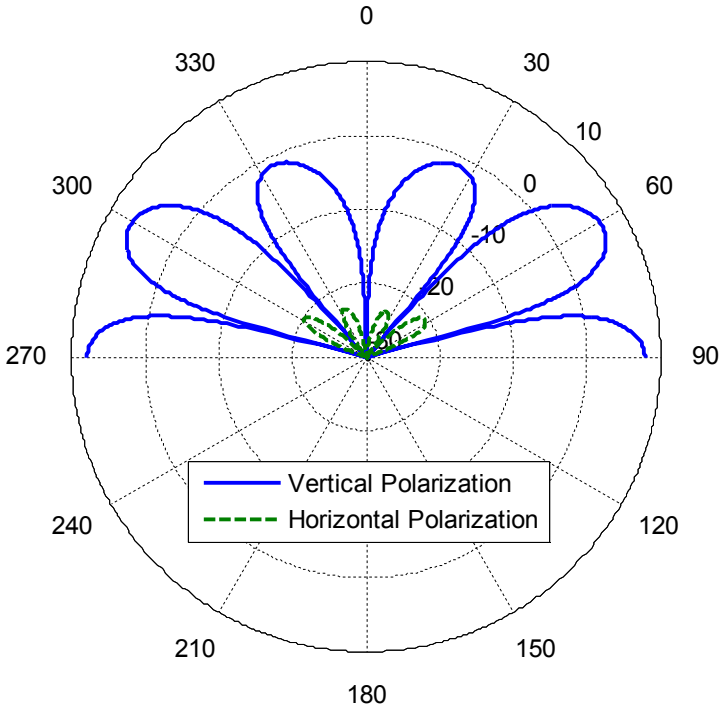

(d)

Figure 25: Geometry and electrical characteristics of an antenna with *ka*=0.2626 for ground separation *kh*=2π. (a) The 4-arm spherical helix antenna. (b) Resistance with

respect to frequency. (c) Reactance with respect to frequency. (d) Radiation pattern at f=300 MHz.

3. Antenna size ka=0.5 and resonant frequency f=571 MHz

3.1 kh=1

Table 9: The resonant 2-arm helix antenna's properties above a PEC ground plane.

Number of Arms	Number of Turns	Total Wire Length (cm)	Number of Sections of a Arm	Q_{gnd}^{imp}
2	0.68	30.3156	48	12.71

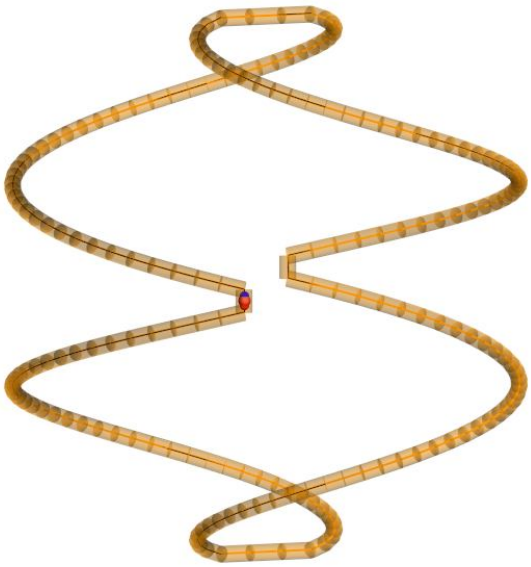

(a)

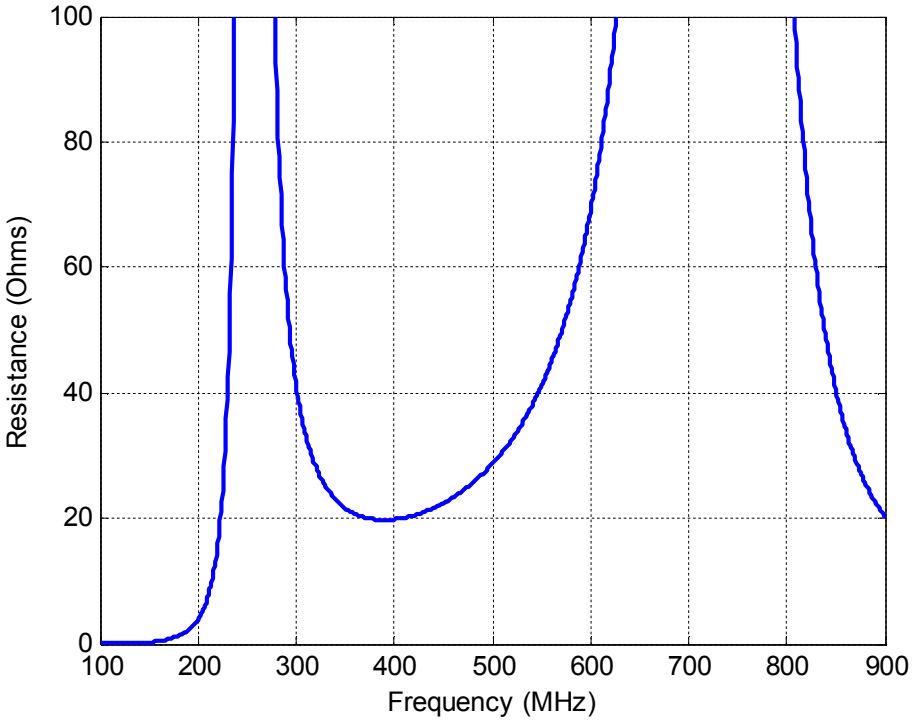
Resistance (Ohms)
Frequency (MHz)
0
20
40
60
80
100
100
200
300
400
500
600
700
800
900

(b)

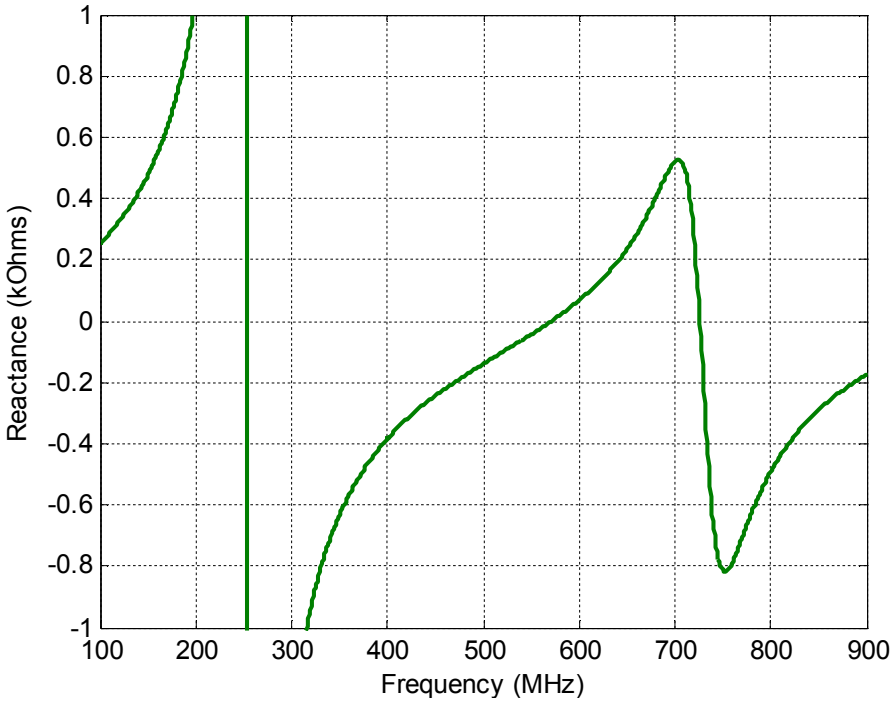
Reactance (kOhms)
Frequency (MHz)
1
0.8
0.6
0.4
0.2
0
-0.2
-0.4
-0.6
-0.8
-1
100
200
300
400
500
600
700
800
900

(c)

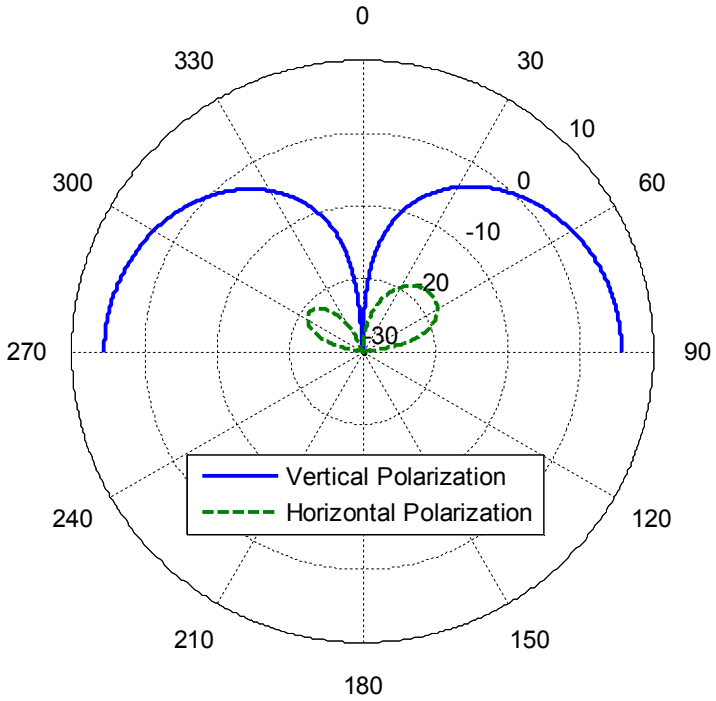

(d)

Figure 26: Geometry and electrical characteristics of an antenna with ka=0.5 for ground separation kh=1. (a) The 2-arm spherical helix antenna. (b) Resistance with respect to frequency. (c) Reactance with respect to frequency. (d) Radiation pattern at f=571 MHz.

3.2 $kh=\frac{1}{2}\pi$

Table 10: The resonant 2-arm antenna's properties above a PEC ground plane.

Number of Arms	Number of Turns	Total Wire Length (cm)	Number of Sections of a Arm	Q_{gnd}^{imp}
2	0.6954	30.8674	48	16.22

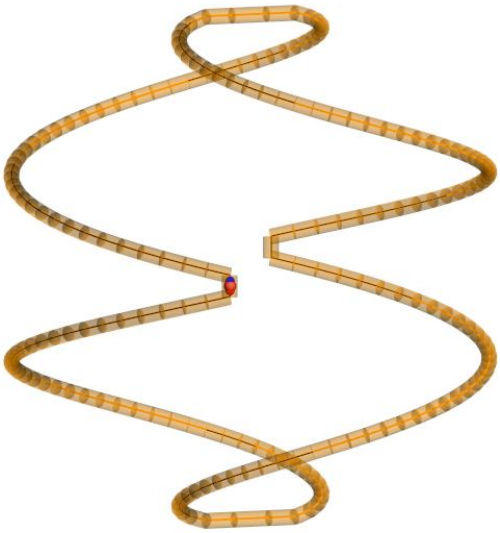

(a)

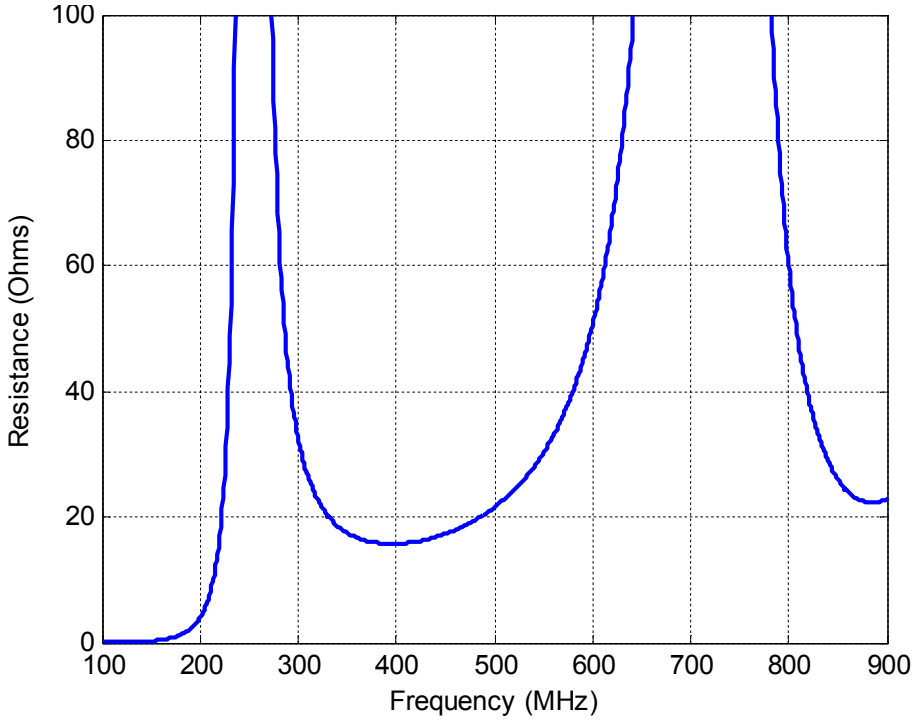
Resistance (Ohms)
Frequency (MHz)
0
20
40
60
80
100
100
200
300
400
500
600
700
800
900

(b)

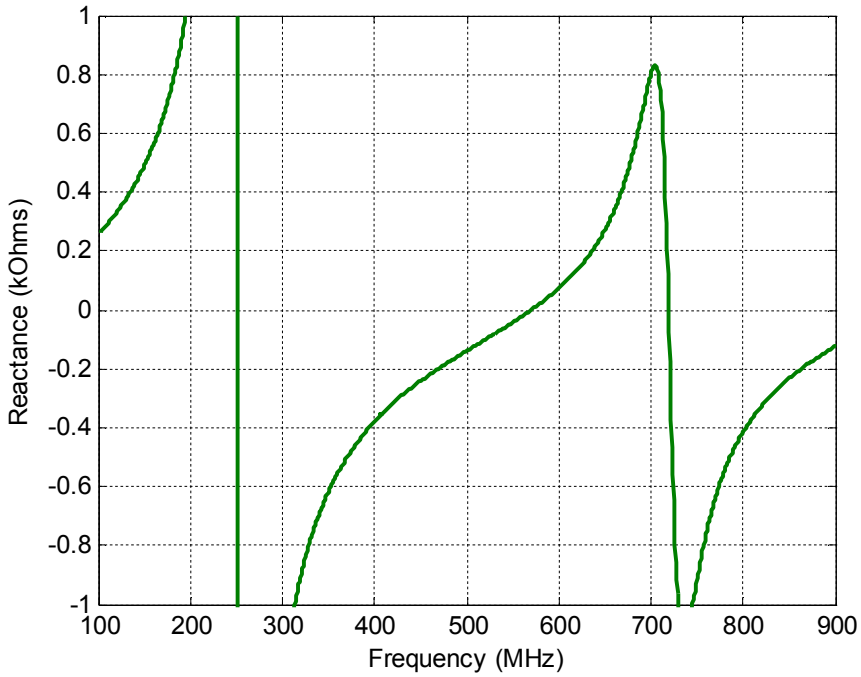

(c)

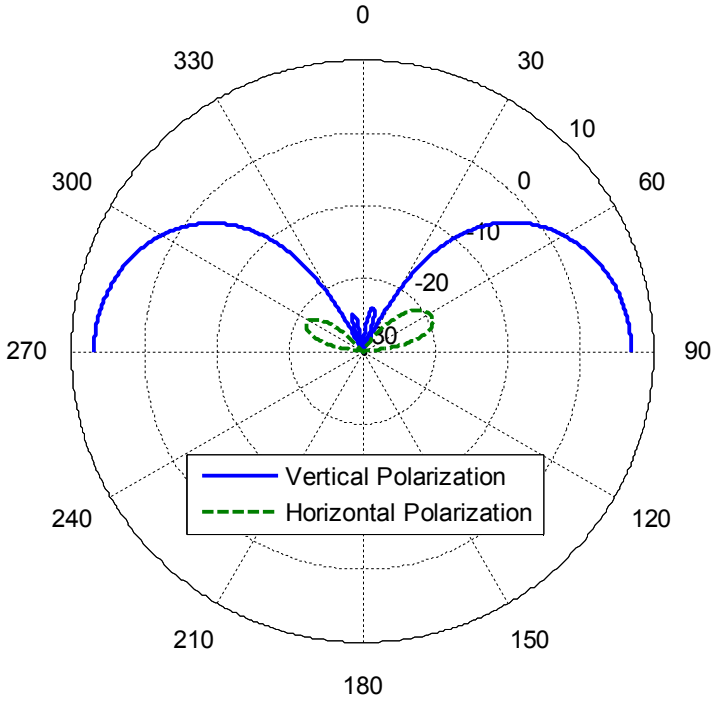

(d)

Figure 27: Geometry and electrical characteristics of an antenna with ka=0.5 for ground separation kh=0.5π. (a) The 2-arm spherical helix antenna. (b) Resistance with respect to frequency. (c) Reactance with respect to frequency. (d) Radiation pattern at f=571 MHz.

3.3 $kh=\pi$

Table 11: The resonant 2-arm helix antenna's properties above a PEC ground plane.

Number of Arms	Number of Turns	Total Wire Length (cm)	Number of Sections of a Arm	Q_{gnd}^{imp}
2	0.68	30.3156	48	18.60

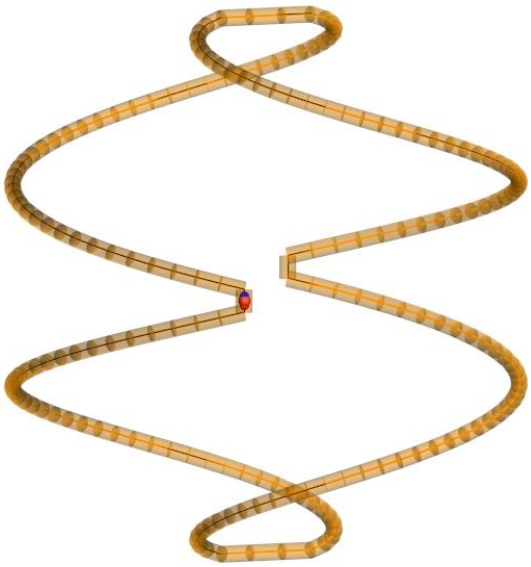

(a)

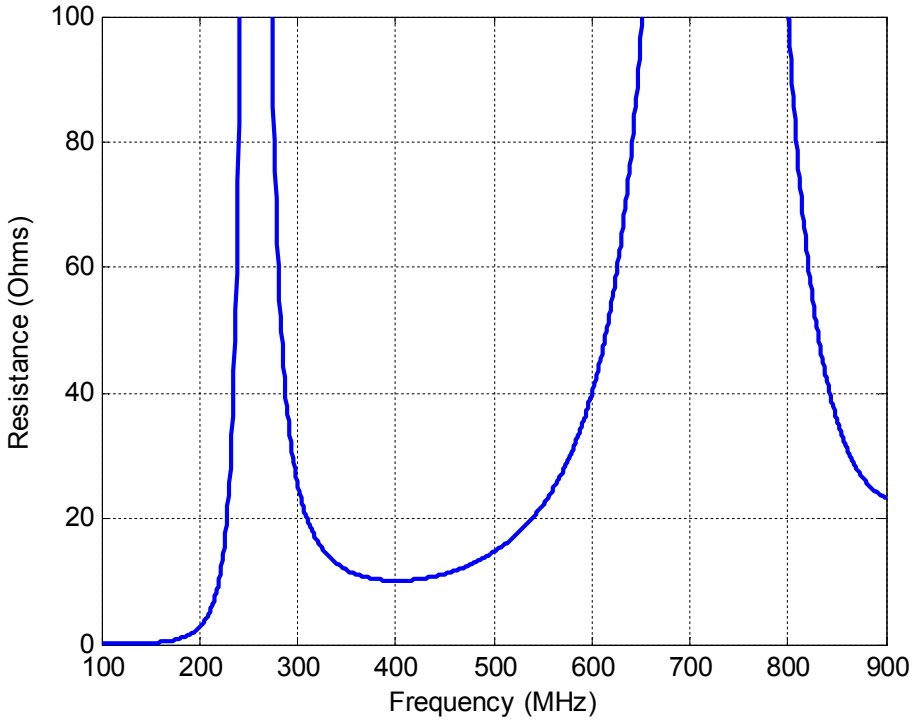
Resistance (Ohms)
Frequency (MHz)
0
20
40
60
80
100
100
200
300
400
500
600
700
800
900

(b)

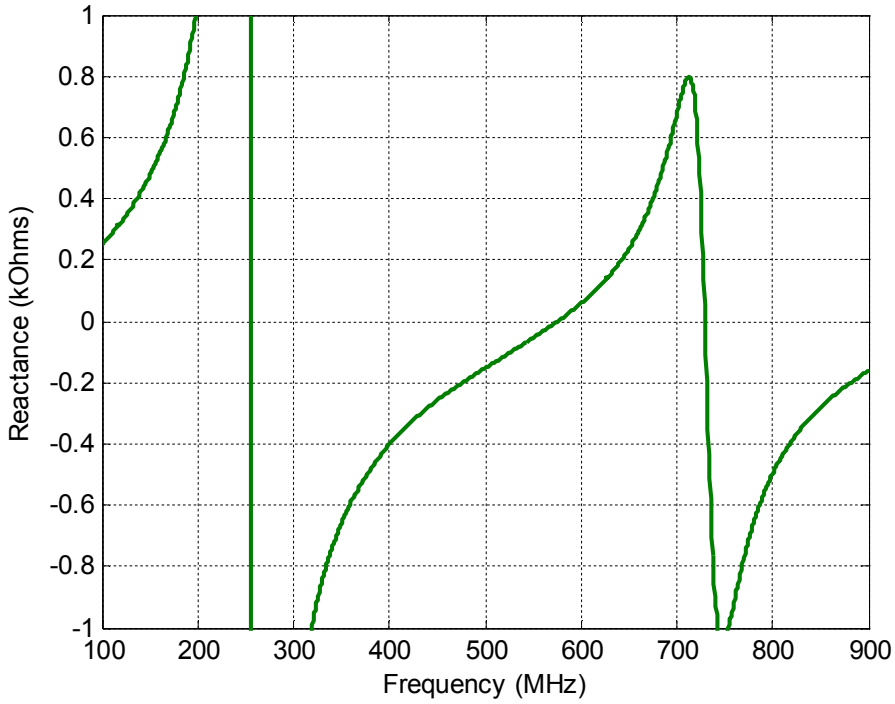
Reactance (kOhms)
Frequency (MHz)
1
0.8
0.6
0.4
0.2
0
-0.2
-0.4
-0.6
-0.8
-1
100
200
300
400
500
600
700
800
900

(c)

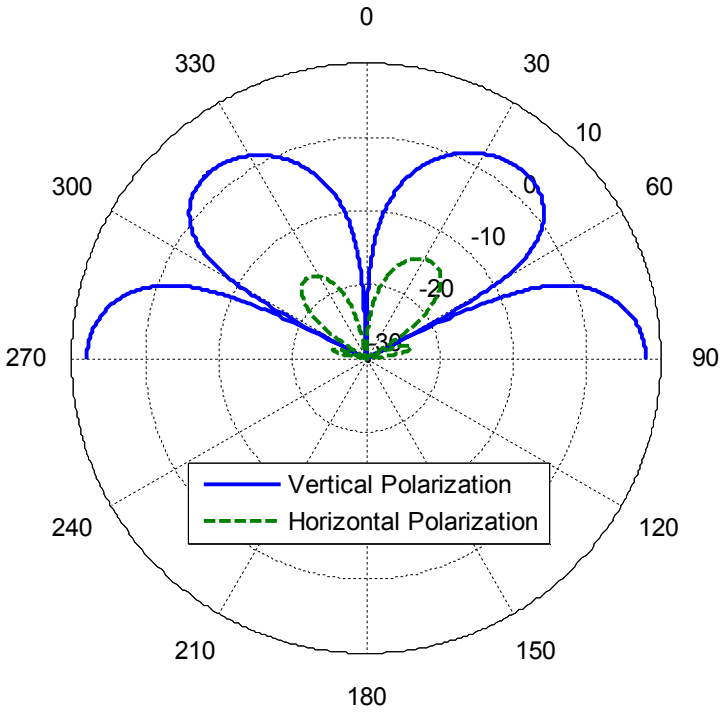

(d)

Figure 28: Geometry and electrical characteristics of an antenna with ka=0.5 for ground separation kh=π. (a) The 2-arm spherical helix antenna. (b) Resistance with respect to frequency. (c) Reactance with respect to frequency. (d) Radiation pattern at f=571 MHz.

3.4 kh=2π

Table 12: The resonant 2-arm helix antenna's properties above a PEC ground plane.

Number of Arms	Number of Turns	Total Wire Length (cm)	Number of Sections of a Arm	Q_{gnd}^{imp}
2	0.68	30.3156	48	19.03

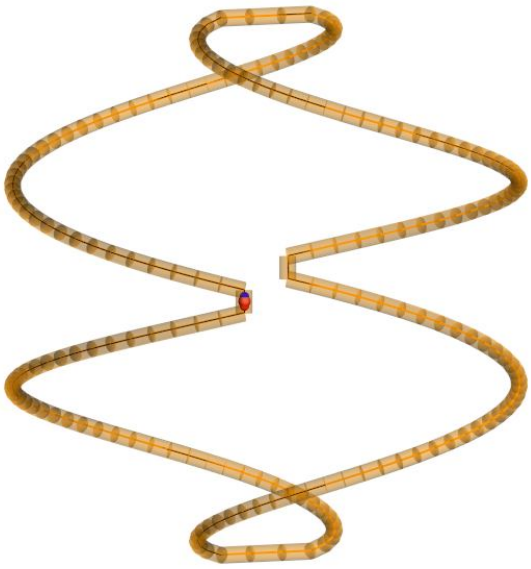

(a)

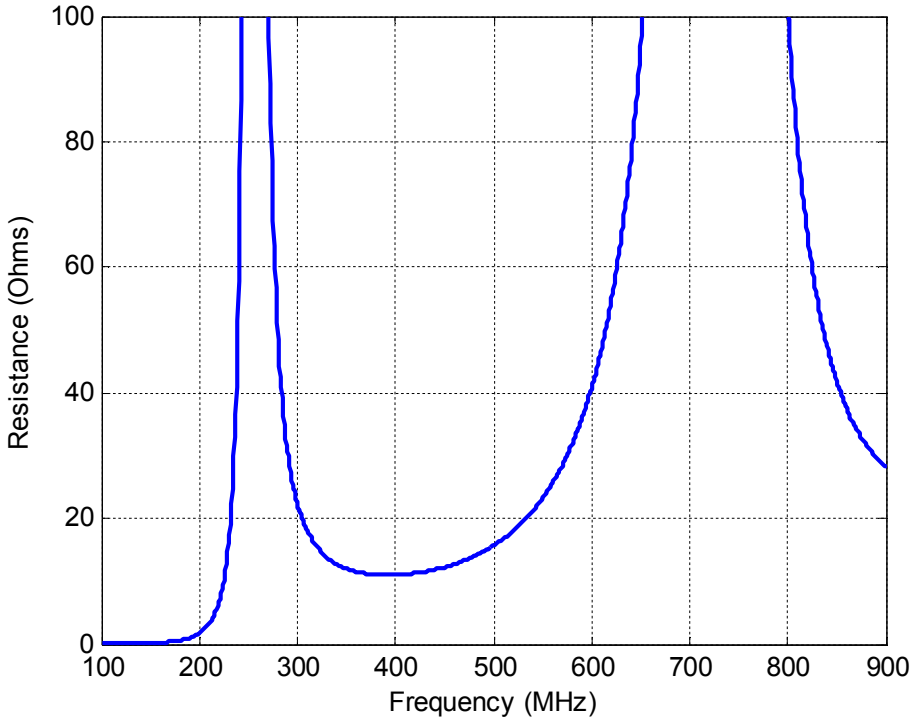
Resistance (Ohms)
Frequency (MHz)
0
20
40
60
80
100
100
200
300
400
500
600
700
800
900

(b)

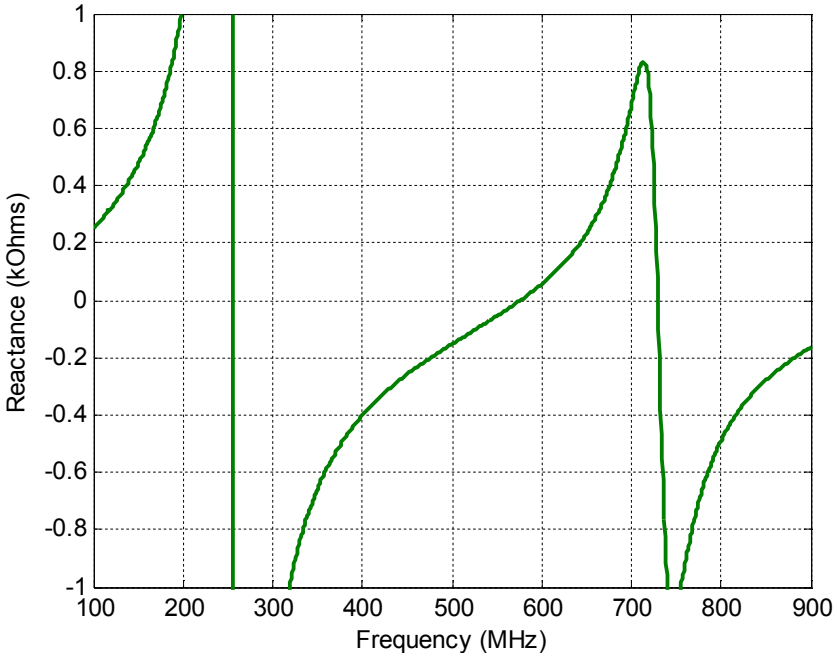

(c)

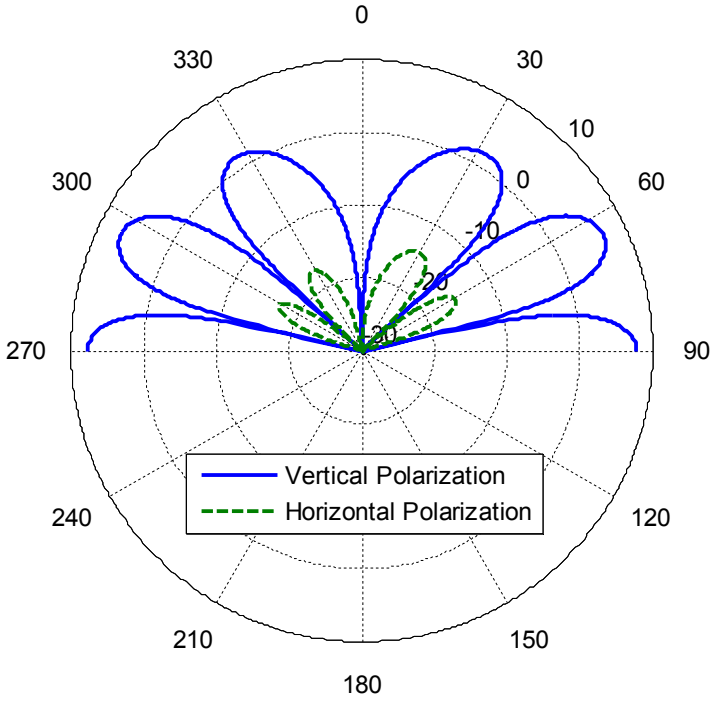

(d)

Figure 29: Geometry and electrical characteristics of an antenna with *ka*=0.5 for ground separation *kh*=2π. (a) The 2-arm spherical helix antenna. (b) Resistance with respect to frequency. (c) Reactance with respect to frequency. (d) Radiation pattern at *f*=571 MHz.

BIBLIOGRAPHY

[1] H. A. Wheeler, "Fundamental limitations of small antenna," *Proceedings of the IRE*, vol. 35, pp. 1479-1484, Dec. 1937.

[2] L. J. Chu, "Physical limitations of omni-directional antennas," *Journal of Applied Physics*, vol. 19, pp. 1163-1175, Dec. 1948.

[3] O. S. Kim, "Electrically small magnetic dipole antennas with quality factors approaching the Chu lower bound," *IEEE Antennas and Propagation,* vol. 58, no. 6, pp. 1898-1906, June 2010.

[4] O. S. Kim, "Minimum Q electrically small spherical magnetic dipole antenna-practice," in *Proceedings of the International Symposium on Antennas and Propagation*, Bangkok, Thailand, Oct. 2009, pp. 89-92.

[5] H. L. Thal, "New radiation Q limits for spherical wire antennas," *IEEE Transactions on Antennas and Propagation*, vol. 54, no. 10, pp. 2757-2763, Oct. 2006.

[6] R. C. Hansen and R. E. Collin, "A new Chu formula for Q," *IEEE Antennas and Propagation Magazine*, vol. 51, no. 5, pp. 38-41, Oct. 2009.

[7] S. R. Best, "Low Q electrically small linear and elliptical polarized spherical dipole antenna," *IEEE Transactions on Antennas and Propagation*, vol. 3, no. 3, pp. 1047-1053, Mar. 2005.

[8] S. R. Best, "The radiation properties of electrically small folded spherical helix antennas," *IEEE Transactions on Antennas and Propagation*, vol. 52, no. 4, pp. 953-960, Apr. 2004.

[9] A. D. Yaghjian and S. R. Best, "Impedance, bandwidth and Q of antennas," *IEEE Transactions on Antennas and Propagation*, vol.53, no. 4, pp. 1298-1324, Apr. 2005.

[10] J. C.-E. Sten, A. Hujanen, and P. K. Koivisto, "Quality factor of an electrically small antenna radiating close to a conducting plane," *IEEE Transactions on Antennas Propagation*, vol. 49, no. 5, pp.829-837, May 2001.

[11] J. A. Stratton, *Electromagnetic Theory*, New York, NY: McGraw-Hill, 1941.

[12] J. E. Hansen, *Spherical Near-Field Antenna Measurements*, London: Peter Peregrinus, 1988.

[13] D.-H. Kwon and D. M. Pozar, "Optimal characteristics of an arbitrary receive antenna," *IEEE Transactions on Antennas and Propagation*, vol. 57, no. 12, pp. 3720-3727, Dec. 2009.

[14] O. R. Cruzan, "Translational addition theorems for spherical vector wave functions," *Quarterly of Applied Mathematics*, vol. 20, no. 1, pp. 33-40, 1962.

[15] S. Stein, "Addition theorem for spherical wave functions," *Quarterly of Applied Mathematics,* vol. 19, pp. 15-24, 1961.

[16] R. E. Collin and S. Rothschild, "Evaluation of antenna Q," *IEEE Transactions on Antennas Propagation*, vol. 12, no. 1, pp. 23-27, Jan. 1964.

[17] R. L. Fante, "Quality factor of general ideal antennas", *IEEE Transactions on Antennas Propagation*, vol. 17, no. 2, pp.151-155, Mar. 1960.